Article

Assessment of Complex Terminal Groundwater Aquifer for Different Use of Oued Souf Valley (Algeria) Using Multivariate Statistical Methods, Geostatistical Modeling, and Water Quality Index

Ayoub Barkat [1,*], Foued Bouaicha [2], Oualid Bouteraa [2,3], Tamás Mester [1], Behnam Ata [4], Dániel Balla [5], Zakaria Rahal [6] and György Szabó [1]

1   Department of Landscape Protection and Environmental Geography, University of Debrecen, 4032 Debrecen, Hungary; mester.tamas@science.unideb.hu (T.M.); szabo.gyorgy@science.unideb.hu (G.S.)
2   Laboratory of Geology and Environment (LGE), Université Frères Mentouri Constantine, Constantine 25020, Algeria; fouedbouaicha@gmail.com (F.B.); Oualid.bouteraa25@gmail.com (O.B.)
3   Department of Natural and Life Sciences, Mohamed Boudiaf University, M'sila 28000, Algeria
4   Department of Social Geography and Regional Development, University of Debrecen, 4023 Debrecen, Hungary; behnam.ata@science.unideb.hu
5   Department of Computer Graphics and Image Processing, University of Debrecen, 4023 Debrecen, Hungary; balla.daniel@inf.unideb.hu
6   Department of Water Supply and Sanitation, Don State Technical University, 344000 Rostov-on-Don, Russia; zakariarhl@yahoo.com
*   Correspondence: ayoub.barkat@science.unideb.hu; Tel.: +36-30-907-5828 (ext. 4032)

Abstract: This research aims to assess the hydrogeochemical evolution of the groundwater in Oued souf valley for drinking and irrigation purposes. To achieve this, 49 groundwater samples from the complex terminal were examined and treated concurrently with multivariate statistical methods, geostatistical modeling and the *WQI* (water quality index). Focusing on the physico-chemical parameters, Q mode clustering analysis detected four major water groups, where the mineralization augmented from group 1 to group 4. The hydro-chemical type was the same, Ca-Mg-Cl-SO_4 for all the groups. Calcite, dolomite, anhydrite, and gypsum would be the dominant reactions with the undersaturation of evaporates minerals, based on geochemical modeling, while the carbonate minerals are precipitating. Geostatistical analysis using ordinary Kriging demonstrated the exponential semi-variogram model fitted for EC (electrical conductivity), Ca^{2+} (calcium), Mg^{2+} (magnesium), K^+ (potassium), HCO_3^- (bicarbonate), Cl^- (chloride), and SO_4^{2-} (sulfate). At the same time, the rational quadratic model was the best-fitted semi-variogram model for Na^+ (sodium) and NO_3^- (nitrate). EC, SO_4^{2-}, and NO_3^- have a strong spatial structure, while Ca^{2+}, Na^+, K^+, and HCO_3^- have a moderate spatial structure. Moreover, there was a weak spatial structure for Mg^{2+} and Cl^-. The WQI shows that CT (complex terminal groundwater aquifers) are not suitable for drinking and their quality for irrigation fluctuates from excellent to moderate quality.

Keywords: complex terminal aquifer; water–rock interaction; multivariate statistical methods; geostatistics; geochemical modeling; WQI

1. Introduction

Natural resources are very limited and continuously degraded due to climate change, rapid population growth, poor management, and misunderstanding of the resources' nature caused by the miscoordination and approaches' integration. Among all, water is the primary natural resource and the most vital one, which is responsible for nourishing and productivity functions of any ecosystem. Despite this natural resource being limited spatially and temporally to humans and other living beings, many problems related to its sustainability are due to humankind's competition over it [1].

A country such as Algeria receives approximately 90 billion m3 of rain per year, 85% of which evaporates, and the rest seeps into the ground [2]. In terms of groundwater resources, the exploited volume is estimated at 1.8 billion m3 in the northern part of the country, which is almost fully utilized nowadays [3]. However, the Oued souf region is located in the country's south, in the northeast part of the enormous desert known as the "Algerian Sahara", which is one of the country's greatest deserts. Groundwater is the only source for drinking and agricultural water in the Oued souf region.

Huge groundwater reserves are stored in this region, which are discovered in the form of aquifers encased in geological horizons of varying depths and thickness. The Oued souf area is defined by the top-to-bottom superposition of three groundwater aquifers, which are part of the northern Sahara aquifer system. The north Sahara aquifer system is composed of three groundwater aquifers, the superficial aquifer or free groundwater aquifer, the complex terminal aquifer, and the continental intercalary groundwater aquifer, where the last two aquifers contain several water layers superimposed on one another. Furthermore, they represent one of the largest hydraulic reservoirs globally, where the mobilizable potentialities are estimated at 5 billion m3 of water [4,5].

Despite the richness of this region in groundwater, it presents low to bad water quality. The superficial aquifer has become less used (20 years ago) because of its excessive mineralization and high pollution degree, either mineral or organic. Moreover, it confronted rising of the water table, which resulted in negative impacts on the public and environmental scope. Since the Oued Souf region is characterized by scarcity of precipitation and swift population growth, it applies high pressure on water demand for drinking water supply, irrigation, and the industry. Due to the relatively bearable cost of drilling with an extensive pumping of 70.34 cubic hectometers in 1999 to 116.27 cubic hectometers in 2013, recent drillings have been oriented towards deep groundwater aquifers, from complex terminal and continental intercalary, either for drinking or irrigation purposes [6].

Northern Sahara of Algeria has been the subject of research in several studies, that have mainly highlighted on the geological and hydrogeological contexts of their aquifers, in reconnaissance of the northern Sahara aquifer system [7–13]. In addition to geological and hydrogeological studies, various studies undertaken over the past thirty plus years have shown that the groundwater's quality of this region is characterized by excessive total mineralization, most often associated with high hardness and high fluoride concentrations, which often exceed the guide values recommended by the World Health Organization (WHO) and values of Algerian limits using conventional methods hydro-chemically, statistically, and even using isotopic methods [14–23]. Other studies focused on the treatment of these groundwaters using different techniques, such as lime precipitation and electrocoagulation using bipolar aluminum electrodes and activated natural materials [24–26].

The variation of the lithological, hydrodynamic, and hydro-chemical conditions in the Oued souf groundwater aquifers conferred a particular interest in its aquifers, especially the complex terminal aquifer, which is the most exploited for domestic and irrigation uses. Despite all the complexities, we believe in the existence of controlling factors that dominate the chemical composition of the complex terminal groundwater aquifer in Oued souf valley. Based on this hypothesis, HCA (Q-mode hierarchical clustering analysis), geostatistics, and the WQI (water quality index) have been used in this study for the first time as a complex method for the spatial explanation of different ions' distribution and the composition changes with the lithological variations of the host rock.

2. Materials and Methods

2.1. Site Description

Oued souf valley lies in the southeast of Algeria. It is common that Oued souf valley is referred to as low-lying-Sahara because of its low altitude in a central, large synclinal basin. Historically, it became a municipality in 1957 and has been an official province since 1984. Today, the Oued souf valley covers an area of 11,738 km^2 divided into 18 municipalities, with 41.41 habitants/km^2 according to the National Statistics Office

during 2015. The Republic of Tunisia limits Oued souf valley to the east and Tébessa province to the northeast, Biskra and Khenchla to the North, and Biskra to the northwest. Meanwhile, it is bordered by Djelfa and Ouargla to the west and southwest, respectively. Geographically, Oued souf is, approximately, located between Longitudes X1 = 05°30′, X2 = 07°00′ East, and Latitudes Y1 = 35°30′, Y2 = 37°00′ North. The study area is a part of Oued souf province that spreads over seven municipalities (El Oued, Debila, Guemar, Kouinine, Ourmas, Reguiba, Taghzout) (Figure 1).
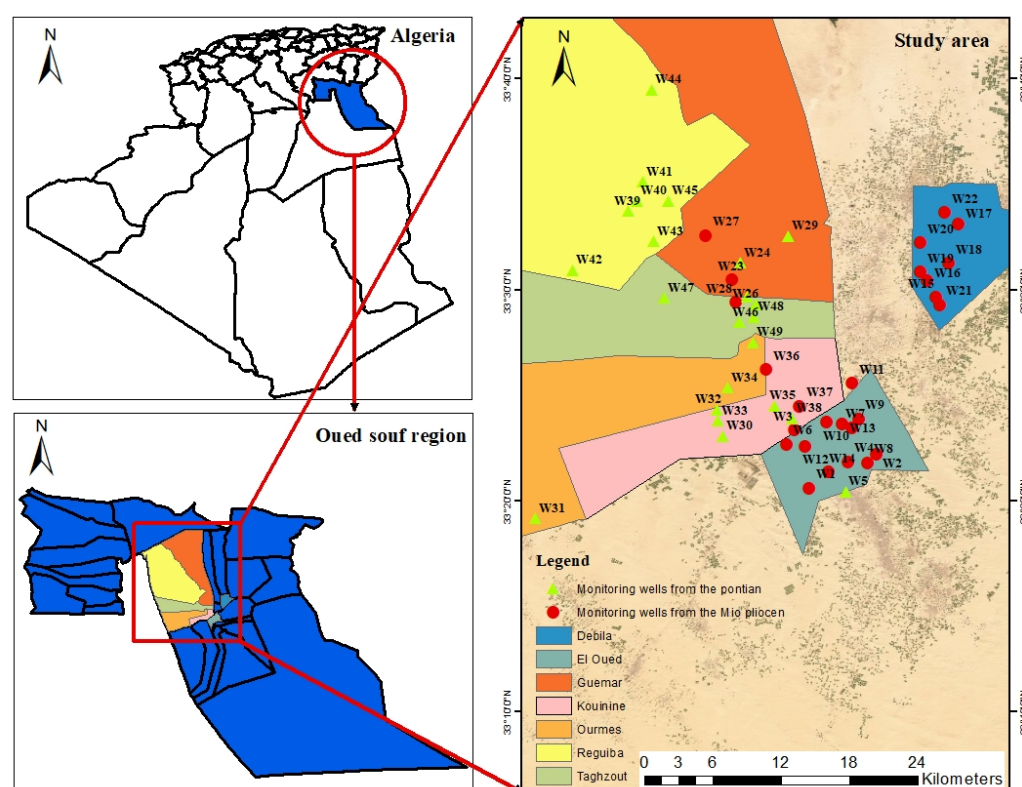

Figure 1. Location map of the study area illustrating the distribution of the monitoring wells.

The main agricultural activity in the Oued souf valley, depicted by a land use/land cover map published in [27], is irrigated agriculture, especially palm tree cultivation. However, in recent years, agriculture in Oued souf has extended to include other crops, such as pivot-irrigated potatoes [28], olives, maize, and other varieties of vegetables. However, all of these crops are irrigated from the uppermost aquifer (water table or phreatic aquifer) that runs underneath the entire Oued souf field. The local farmers have created an original method for palm tree cultivation called ghouts, which consists of digging on the dune's vast basins in which the palm trees are planted and consequently using the phreatic groundwater aquifer for growing. The majority of the existing crops need vast quantities of fertilizers and increased production, influencing groundwater quality. The potential source of pollution can also be represented by the urban areas that have been spreading since 1972. Consequently, the increase of wastewater discharges contributes to groundwater pollution [29]. However, to meet the needs for drinking water and irrigation due to the economic and demographic development of the region, intensive pumping was applied on deep groundwater aquifers (complex terminal and continental intercalary) for different uses, but without sufficient treatment and discharge, these quantities return to the phreatic aquifer [30].

To save the region, it was necessary for the Algerian authorities to release a megaproject to stop the rising groundwater, however this project failed due to several problems [31]. The Oued souf region is diversified between a hot and dry summer and a mild winter, making it very similar to other regions of the Algerian Sahara [32]. The rainfall is typi-

fied by low, oscillatory, and infrequent precipitation, with an annual average of 5.90 mm, according to statistical analysis of meteorological data gathered from the meteorological station of Oued souf airport between 1978 and 2016. Evaporation, with an annual average of 181.18 mm, greatly outnumbers rainfall. The region's average maximum temperatures range from 20.76 °C in January to 45.31 °C in July, with average minimum temperatures ranging from 9.62 °C in January to 30.18 °C in August.

2.2. Geology and Hydrogeology

The Oued souf valley can be described as a synclinal layer formed on a pre-Cambrian tucked basement and filled discordantly by thick Meso-Cenozoic sedimentary formations, and ultimately by detrital, carbonate, or evaporate deposits. However, all of these sedimentary deposits are surrounded by dunes and are pebbly or gravely. Meanwhile, these formations are known as the eastern part of the Great Oriental Erg.

The tormented reliefs of the Great Oriental Erg are found on the basis of a quaternary structure made up of a number of dense and homogeneous tens of meters of eolian sand. This structure comprises the water table, with a descending substratum forwarded to the north. The groundwater of this formation with superficial runoff is expanding in the salty soil lagoons, where it will be evaporated and deposited as a superficial salt crust [8].

Lithostratigraphically, the study area consists primarily of limestone, marly clays, marls, gypsiferous marly clays, and gypsiferous marly clays with lagunal facies on top, from the Cretaceous to the Eocene (gypsum, anhydride, salts, and dolomitic passages). All of this is topped by the Neogene, which is composed of Oligocene conglomerates and shale, as well as Mio-Pliocene sub-horizontal red sandy clays and gypsiferous sandstone lentils. Meanwhile, Plio-Quaternary fine sands with limestone crusts cover everything in a single layer [33]. Furthermore, these sands contain 90% quartz crystals, gypsum, and silicates such as Feldspars and silicate accessories such as epidote zircon, rutile, tourmaline, and garnet, as well as limestone concretions; as a result, they are formatting the possible aquifer (Figure 2) [34,35].
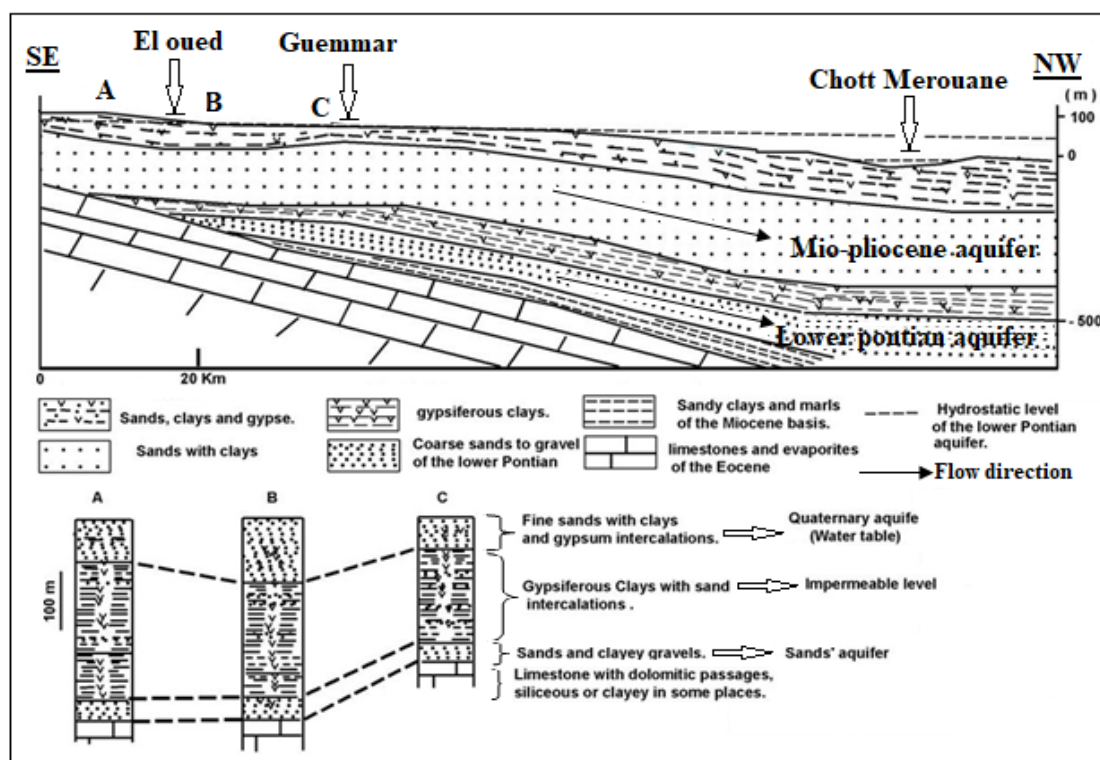

Figure 2. Top: Hydrogeological cross-section of Oued souf valley, bottom: (**A–C**) are log correlation of Oued souf valley modified from [15].

In terms of hydrogeology, the geomorphology and sedimentation of the basin have intensified permeation and subterranean flow of precipitated water on outcrops of concentric halos across the periphery. The alternation of permeable and impermeable deposits ensured their charging as they flowed into the depressed regions. Favorable paleogeographic and geological conditions that occurred during ancient rainy cycles are the factors that contributed to groundwater formation [34]. The continental intercalary aquifer (CI), the terminal continental or complex terminal aquifers (CT), including the limestone aquifer (Senonian-Eocene), sand aquifer (Mio-Pliocene), and quaternary aquifer or water table, are the aquifers of Oued souf valley.

2.3. Piezometry

According to the data obtained from Agence Nationale des Ressources Hydraulique (ANRH) during 2015–2016, the covered study area is drilled by 49 wells, three of which are intended for irrigation and are located in the central city of El Oued, while the others are designed for drinking water supply, spreading over the other covered study area. However, 26 wells are from the Mio-Pliocene aquifer and 23 wells are from the Pontian aquifer. The most bottomless well is located in Guemmar municipality, with a depth of 398 m. This well belongs to the Mio-Pliocene aquifer. Additionally, the lower depth is 265 m in the same municipality, intended for drinking water. In the covered study area, the total abstraction is 67,820,480.64 m^3/year.

In contrast, the biggest extraction is in W25, located in Guemmar for drinking water supply but from the Pontian aquifer. According to the piezometric map illustrated in Figure 3, the overexploitation of the complex terminal aquifer is represented by a high groundwater level in different municipalities and is clearly noted in the south to the middle part of the study area, in El Oued, Bayadha, Mih ouensa, Hassi khalfa, and Robbah. At the same time, the lowest levels are located in the northern part of the study area, in Magrane, Debila, Reguiba, and Guemmar. The piezometric level shows that the flow direction is from the south (recharge area) to the north (discharge area), towards Chott Melrhir and Chott Merouane in the north of the study area.
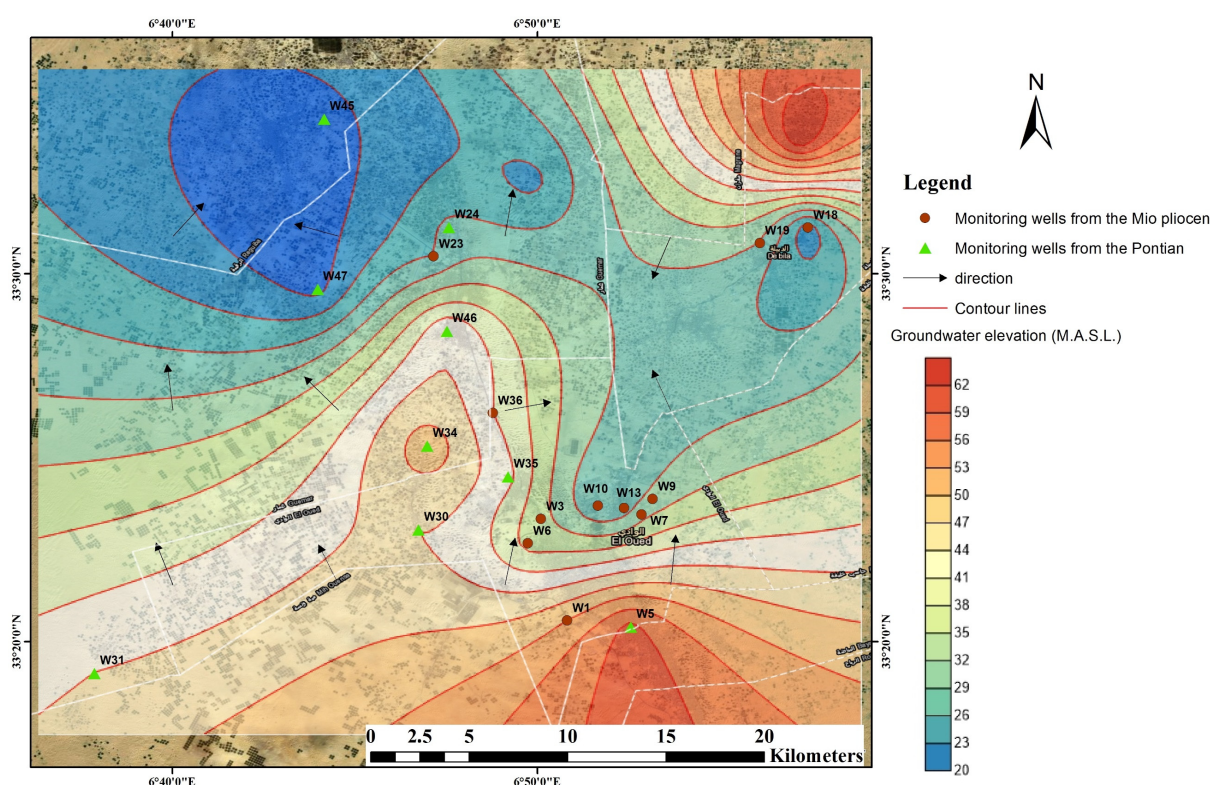

Figure 3. Piezometric map and groundwater flow of the complex terminal aquifer.

2.4. Sampling and Analysis

Forty-nine (49) groundwater samples were collected and analyzed by Agence Nationale des Ressources Hydrauliques (ANRH) of Oued souf from the complex terminal aquifer of the Oued souf region during March 2019 (precisely, El Oued, Debila, Guemar, Kouinine, Ourmas, Reguiba, and Taghzout), including 26 groundwater samples from Mio-Pliocene aquifers and 23 samples from the Pontian, where these wells are intended for domestic and agricultural use. The sampling took place in March of this year. After a brief pumping time in polyethene bottles, the procedure was carried out. The physical parameters temperature, electrical conductivity, and pH were recorded on-site using a Multi–350 i. Multi–parameters. Analyses of the elements Cl^- (chloride), HCO_3^- (bicarbonate), SO_4^{2-} (sulphate), Ca^{2+} (calcium), Mg^{2+} (magnesium), Na^+ (sodium), K^+ (potassium), and NO_3^- (nitrate) were performed by volumetry, UV-visible spectrometry, and flame spectrophotometry [36].

The validation of the analytical results has been carried out by the calculation of the charge balance errors (%E), which was <5% with a negative value, indicating the dominance of the anions in our groundwater samples. Microbiological analyses have also been performed by ANRH, including several parameters such as total germs, total and fecal coliforms, fecal streptococci, and clostridium sulfito reductor, with different areas for the cultivation.

2.5. Clustering Analysis

A method for classifying cases or variables based on their variance or resemblance is hierarchical cluster analysis. It is widely used, particularly for hydrochemistry investigations, to classify hydrogeochemical processes in groundwater by clustering collected water samples into distinct groups important in the geological and hydrogeological sense. Furthermore, this unsupervised grouping will distinguish water quality variables based on their similarity. Euclidean distances were used to classify parameters into initial clusters, whilst Ward's agglomeration method was used to link the resulting initial clusters [37–43].

2.6. Hydro-Chemical Analysis

The hydro-chemical recognition was performed by constructing diagrams such as the Piper diagram [44] and Chadha diagram [45], while Gibbs diagram [46] was also used to identify the main mechanisms governing the chemistry of groundwater.

2.7. Geostatistical Modeling

Geographical information system (GIS) applications are helpful tools to find the spatial distribution of groundwater quality parameters by integrating spatial data with other information to facilitate environmental protection and resource planning [47,48], and also for the evaluation of groundwater quality by the intervention of geostatistics [49,50]. Geostatistics is a mathematical tool concerned with spatial correlation schemes and the variogram, a quantitative spatial correlation measure commonly used in geostatistics [51]. Meanwhile, interpolation techniques such as Kriging will provide a neutral, best linear approximation of a regionalized vector in non-sampled locations [52–54].

Kriging, which can approximate the interpolation error of the values of the regionalized variable where there are no original measurements, is one of the best methods in geostatistics for interpolation at unsampled sites. Kriging is a method for estimating the spatial distribution of a variable's reliability and precision. A semi-variogram, which is mathematically defined by the equation below, can be used to quantify spatial dependence:

$$G(h) = \frac{1}{2N(h)} \sum_{i=1}^{N(h)} [Z(Xi+h) - Z(Xi)] \tag{1}$$

γ (h) illustrates the semi-variogram as a function of the lag distance or separation vector, h, between two pints, N (h) represents the number of observation pairs divided by distance, h, and Z (Xi) represents the random variable at position Xi [55].

Ordinary Kriging is a linear appropriate interpolation technique that can produce predictive maps and was available in the ArcGIS (made by Environmental Systems Research Institute (Esri) in United States (California)) geostatistical extension. The spatial distribution, on the other hand, can be determined using the equation below [56]:

$$Z(X0) = \sum_{i=1}^{n} n \ \lambda i \ Z(Xi) \tag{2}$$

where $Z(X0)$ is the predictable value at $X0$ points, while n is the number of the sampled point, $Z(Xi)$ is the recognized value at sampled Xi points, and λ is the weight assigned to the sampled point. The geostatistical analysis was performed using ArcGIS 10.4.1 software for generating spatial distribution maps.

2.8. Assessment for Drinking Purposes

The water quality index is a valuable tool for determining the quality of groundwater and whether it is suitable for drinking or irrigation [57,58]. Water quality index is a rating system that shows the cumulative impact of water quality parameters on total water quality. Furthermore, combining nuanced data and creating a score that describes water quality status is considered a convenient and easy way for decision-makers to gain a deeper understanding of the quality of surface/groundwater sources [59], where its formula is as follows [60]:

$$WQI = \sum_{i=1}^{n} Qi \ Wi \ / \sum_{i=1}^{n} Wi \tag{3}$$

The ith parameter's quality rating is Q_i, and each parameter's W_{unit} weight is n number of parameters.

$$Qi = \left[\frac{Vi - V0}{Si - V0} \right] \tag{4}$$

where Vi is the ith parameter's observed value, $V0$ is the ith parameter's ideal value in pure water, $V0$ is zero for all parameters except pH = 7.0, and Si is the ith parameter's standard permitted value.

Computation of unit weight, Wi, is contrarywise proportionate to the standard permissible value, Si, for water quality parameters:

$$Wi = \frac{K}{Si} \tag{5}$$

where K represents the weights' proportionality constant:

$$K = \frac{1}{\sum_{i=1}^{n} \frac{1}{S}} \tag{6}$$

When the WQI is less than 50, it is called excellent, decent (100–125), bad (125.1–150), very poor (150.1–175), and unfit for drinking when the WQI is greater than 175 (175–200).

2.9. Irrigation Suitability Assessment

The assessment of complex terminal groundwater samples for irrigation usage was performed by different ionic parameters in meq/L based on various indices, such as electrical conductivity (EC) (μS/cm) [61], total hardness (TH) [62], and alkalinity hazard (SAR), which is the fraction of Na+ ions in the water sample to Ca^{2+} and Mg^{2+} ions. As a result of constant usage of sodic water, the SAR is used to assess the potential for Na+ to build in the soil, predominantly (water flow) at the expense of Ca^{2+}, Mg^{2+}, and K^+ [61]. The percent Na is also employed in irrigation water classification. Na^+ is an important

characteristic that aids in the classification of any water source for irrigation purposes. Na^+ binds to the soil chemically, reducing the soil's ability to transfer water. Alkaline soils are formed when Na^+ reacts with CO_3^{2-}, whilst saline soils are formed when Na^+ combines with chloride. Crop development is slowed by sodium-affected soil (alkaline/saline) [63].

Alkaline earths (Ca^{2+} and Mg^{2+}) are usually in a condition of equilibrium in groundwater. Both Ca^{2+} and Mg^{2+} ions are associated with soil friability and aggregation, and both are important nutrients for crop growth. The presence of high concentrations of Ca^{2+} and Mg^{2+} in water can elevate soil pH (converting the soil to a saline state), reducing phosphorus availability. Magnesium in excess in groundwater degrades soil quality by turning it alkaline, resulting in lower agricultural yields. Excess Mg^{2+} ions in water, according to agriculturists, degrade soil quality, resulting in low crop productivity, and this is expressed by MH (magnesium hazard) [64]. The RSC (residual sodium carbonate index) presents the amount of bicarbonate/carbonate and calcium/magnesium in irrigation water. Precipitation of Ca^{2+} and Mg^{2+} occurs when the concentrations of carbonate (CO_3^{2-}) and bicarbonate (HCO_3^-) ions surpass the concentrations of Ca^{2+} and Mg^{2+} ions. It details the leftover $NaCO_3$ that is missing if the carbonates are fewer than alkaline earths ($Ca^{2+} + Mg^{2+}$).

An overabundance of CO_3^{2-} and HCO_3^- causes soil Ca^{2+} and Mg^{2+} to precipitate, affecting soil structure and potentially activating soil sodium [65]. The permeability index (PI) is a metric used to determine whether water is suitable for irrigation. The capacity of soil to transport water (permeability) is influenced by the long-term usage of irrigation water (with a high salt content), as well as the soil's Na^+, Ca^{2+}, Mg^{2+}, and HCO_3^- ions [66]. The KR (Kelley ratio) is another indicator for determining the quality and classification of water for irrigation purposes, which is based on the ratio of Na^+ to Ca^{2+} and Mg^{2+} [67].

All indices are expressed by the following equations:

$$TH = 2.5 \times Ca + 4.1 \times Mg \tag{7}$$

$$\% \, Na = 100 \times \frac{Na + K}{Ca + Mg + Na + K} \tag{8}$$

$$SAR = \frac{Na}{\sqrt{\frac{Ca+Mg}{2}}} \tag{9}$$

$$PI = 100 \times \frac{Na + \sqrt{HCO_3}}{Na + Mg + Ca} \tag{10}$$

$$KR = \frac{Na}{Ca + Mg} \tag{11}$$

$$RSC = (HCO_3 + CO_3) - (Ca + Mg) \tag{12}$$

$$MH = \frac{Mg}{Ca + Mg} \tag{13}$$

2.10. Geochemical Modeling

Geochemical modeling was performed using PHREEQC interactive software (made by United States Geological Survey (USGS) in united states) on our measured data for defining the chemical reactions and aqueous speciation in the aquifer system, and subsequently to assess the equilibrium state among groundwater and the existing minerals relating to the saturation index (*SI*) [68], which is calculated using the following equation:

$$SI = Log\left(\frac{IAP}{Kt}\right) \tag{14}$$

where *SI* is the saturation index of the mineral, while *IAP* is the ion activity product of the dissociated mineral, and *Kt* is equilibrium solubility at mineral temperature. The

groundwater is being under-saturated when *SI* < 0 of a particular mineral (mineral dissolution condition). *SI* > 0 indicates the oversaturation of a particular mineral (precipitation condition), whilst *S* = 0 reflects the equilibrium state. Chloralkaline indices were computed to comprehend the cation exchange process incidence in the study area based on [69] the equations (meq/L):

$$\text{CAI} - \text{I} = \frac{\text{Cl} - (\text{Na} + \text{K})}{\text{Cl}} \tag{15}$$

$$\text{CAI} - \text{II} = \frac{\text{Cl} - (\text{Na} + \text{K})}{\text{Cl}} \tag{16}$$

3. Results and Discussion

3.1. Physicochemical Characterization of Groundwater

Table 1 shows a statistical description of the analyzed physicochemical parameters and measured groundwater samples. Meanwhile, a microbiological examination of the complex terminal groundwater aquifer reveals the absence of microbiological contamination.

Table 1. List of the physicochemical parameters evaluated and calculated in groundwater samples.

Variables	Mean	S.D.	Minimum	Maximum	WHO Standards
T °C	23.11939	5.04642	11.8	35.1	-
pH	7.49	0.15241	7.23	7.84	6.5–8.5
EC (μs/cm)	4131.48	382.9674	2760	4730	1000
Salinity (%)	2.64082	0.25753	1.8	3	-
TDS (mg/L)	2650.918	246.3647	1766	3027	500
Turbidity (Ntu)	0.42989	0.51532	0.074	3.23	5
Dry Residue (mg/L)	3075.102	478.8925	1900	3980	-
Total Alkalinity (mg/L)	138.8674	27.16899	83	189	-
TH (mg/L)	1196.653	111.723	950	1430	-
Ca^{2+} (mg/L)	274.9588	36.84752	200.4	360.72	75
Mg^{2+} (mg/L)	122.7436	30.19053	63.12	184.718	50
Na^+ (mg/L)	379.4082	57.92557	137	600	200
K^+ (mg/L)	33.34694	7.0113	15	50	12
Cl^- (mg/L)	888.5908	144.18	457.343	1240.855	250
SO_4^{2-} (mg/L)	729.0941	152.2067	193.061	997.411	250
HCO_3^- (mg/L)	167.9814	33.50002	101.26	213.58	120
NO_3^- (mg/L)	22.3878	6.62298	1.911	34.9	50

The pH levels range from 7.23 to 7.84, with a mean of 7.49. Whereas, in the study area, 100% of groundwater samples were in the range of 7.2–8.5, meaning low alkaline groundwater type, and all pH values were within the WHO (2011) acceptable range for drinking. The groundwater samples ranged in temperature from 11.8 to 35.1 °C. For the electrical conductivity devoted to the different salts dissolved in the groundwater samples, the results portray that the existence of wide variations of the electrical conductivity varied widely, from 2760 to 4730 μs/cm, the mean is 4131.48 μs/cm, and all the recorded values (100% of groundwater samples) exceeded the WHO standards for drinking purposes. A similar trend is observed for the total dissolved solids (TDS) and salinity. TDS in the study area varied from 1766 to 3027 mg/L, with a mean of 2650.918 mg/L, and 100% of groundwater samples were found to exceed the limit of WHO standards. The dissolved matter forms, which consist of inorganic salts, organic matter, and dissolved gases, are the responsible factors that contribute to TDS. However, TDS can classify the groundwater samples as 100% slightly saline, and all of them exceeded WHO standards for drinking purposes. Additionally, the salinity and dry residue are varied from 1.8% to 3% and from 1900 to 3980 mg/L respectively, and 3075.102 mg/L was the average value.

3.2. Cluster Analysis

All major ions (Ca^{2+}, Mg^{2+}, Na^+, K^+, Cl^-, SO_4^{2-}, HCO_3^-, and NO_3^-), EC, TDS, salinity, TH, TA, turbidity, temperature, and dry residue were regarded on the normalized data to establish potential hydro-chemical groups that occurred in the groundwater samples using hierarchical clustering analysis (Q-mode). To compute the similarity of water samples, Ward's linkage technique and Euclidean distance were used to execute HCA. A dendrogram of spatial HCA was generated in Figure 4.
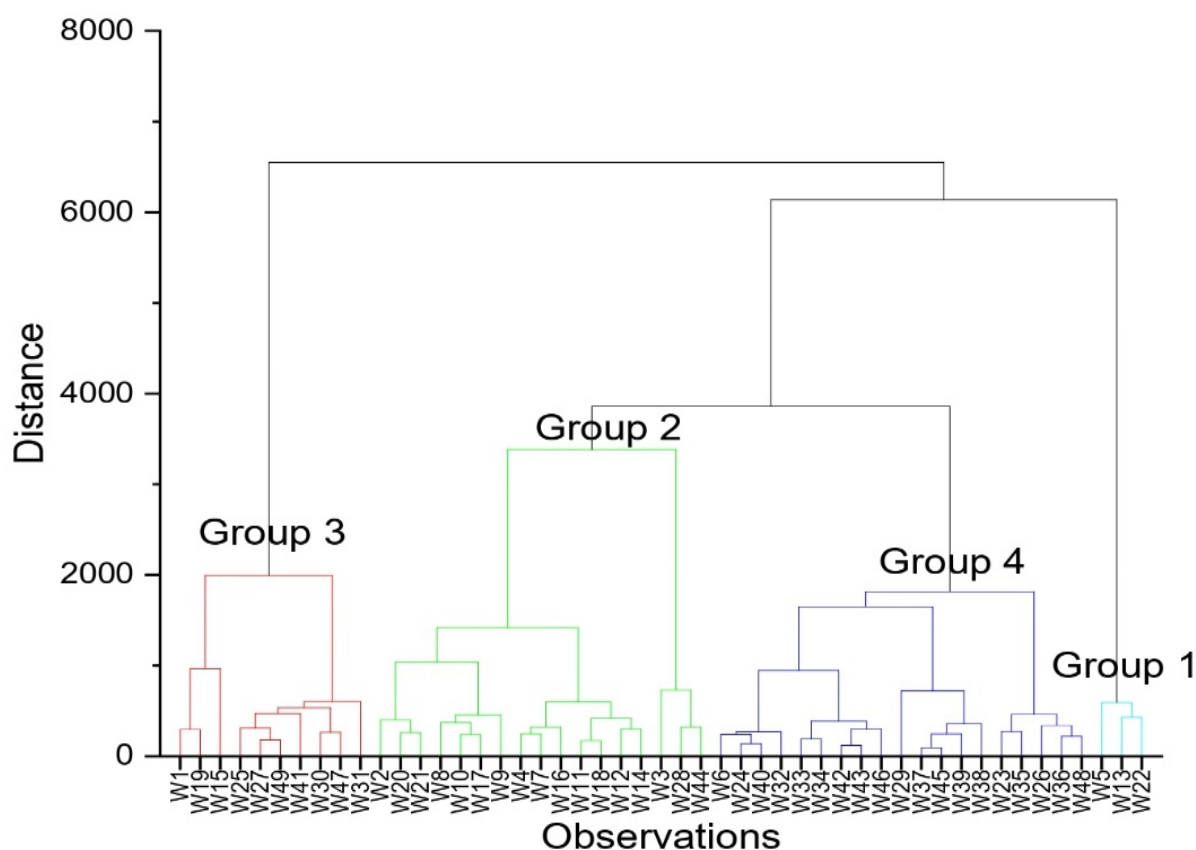

Figure 4. Hierarchical cluster dendrogram—Q mode.

Four groups of groundwater samples were created (Figure 4). The most significant element in distinguishing these classes seems to be EC (Table 2). It is augmenting exponentially from group 1 to group 4. All these groups are plotted in a Piper plot to identify the geochemical evolution of water type. The physicochemical parameters of groundwater groups were compared to the World Health Organization (2011) for drinking water purposes, including statistical analyses.

Hydrochemistry of groundwater aquifers is one of the most difficult to interpret in more or less complex sedimentary environments because of the heterogeneity of the mineralogical chemical properties of the studied area [70]. The average EC of three wells in group 1 (W22, W13, and W5) is 3000 s/cm, indicating considerable mineralization and hence brackish water. A large number of wells are found in the recharge zone and are part of the Mio-Pliocene aquifer. The abundance of major ions is $Na^+ + K^+ > Ca^{2+} > Mg^{2+}$ and $Cl^- > SO_4^{2-} > CO_3^{2-} + HCO_3^- > NO_3^-$, in that order, Figure 5. The hydrochemical facies are characterized by Ca-Mg-Cl-SO_4 type, CaCl type, and chloride type, while one sample is of magnesium type, according to the piper plot in Figure 6. The dominance in this group is devoted to chloride (min = 631.06 mg/L, max = 787.06 mg/L, and mean = 706.7 mg/L), then calcium (min = 240.48 mg/L, max = 280.56 mg/L, and mean = 260.52 mg/L) and magnesium (min = 85.07 mg/L, max = 121.53 mg/L, and

mean = 101.27 mg/L), and sulphates (min = 568.33 mg/L, max = 654.02 mg/L, and mean = 621.57 mg/L). In contrast, the concentration of nitrate has been lower compared to the other elements (min = 1.911 mg/L, max = 34.9 mg/L, and mean = 22.39 mg/L). Chloride, calcium, magnesium, and sulphates exceeded the desirable WHO 2011 standards for drinking water, while nitrate did not exceed the standards.

Table 2. The three main water groups' parameter values.

	Group 1 (*n* = 3)			Group 2 (*n* = 17)			Group 3 (*n* = 10)			Group 4 (*n* = 19)			
	Min	Mean	Max	Min	Mean	Max	Min	Mean	Max	Min	Mean	Max	WHO (2011)
T °C	24.6	28.9	33.1	15.2	22.0	35.1	11.8	21.3	27.4	20.6	24.2	34.0	-
pH	7	8	8	7	8	8	7	7	8	7	7	8	6.5–8.5
EC (µs/cm)	2760	3000	3220	3650	4005	4430	3620	4272	4730	4150	4349	4500	1000
Salinity %	2	2	2	2	3	3	2	3	3	3	3	3	-
TDS (mg/L)	1766	1919	2060	2336	2569	2830	2362	2737	3027	2660	2795	2957	500
Turbidity (NTU)	0	1	1	0	1	3	0	0	0	0	0	1	5
Dry Residue (mg/L)	2320	2440	2520	1900	2818	3420	3480	3728	3980	2560	3062	3480	-
Alkalinity (mg/L)	92	123	150	83	116	168	125	152	170	110	155	189	-
TH (mg/L)	950	1067	1200	1040	1184	1356	1140	1271	1430	960	1189	1330	-
Ca^{2+} (mg/L)	240	261	281	204	263	341	200	283	361	216	284	325	75
Mg^{2+} (mg/L)	85	101	122	63	124	185	63	137	165	66	117	165	50
Na^+ (mg/L)	322	431	600	281	357	410	137	374	460	340	394	420	200
K^+ (mg/L)	32	35	39	15	32	42	32	36	42	22	33	50	12
Cl^- (mg/L)	631	707	787	815	977	1241	457	801	986	730	884	1127	250
SO_4^{2-} (mg/L)	568	622	654	602	764	978	630	818	997	193	668	923	250
HCO_3^- (mg/L)	112	150	183	101	140	205	153	185	207	134	187	214	120
NO_3^- (mg/L)	2	14	20	3	21	30	17	23	29	15	25	35	50
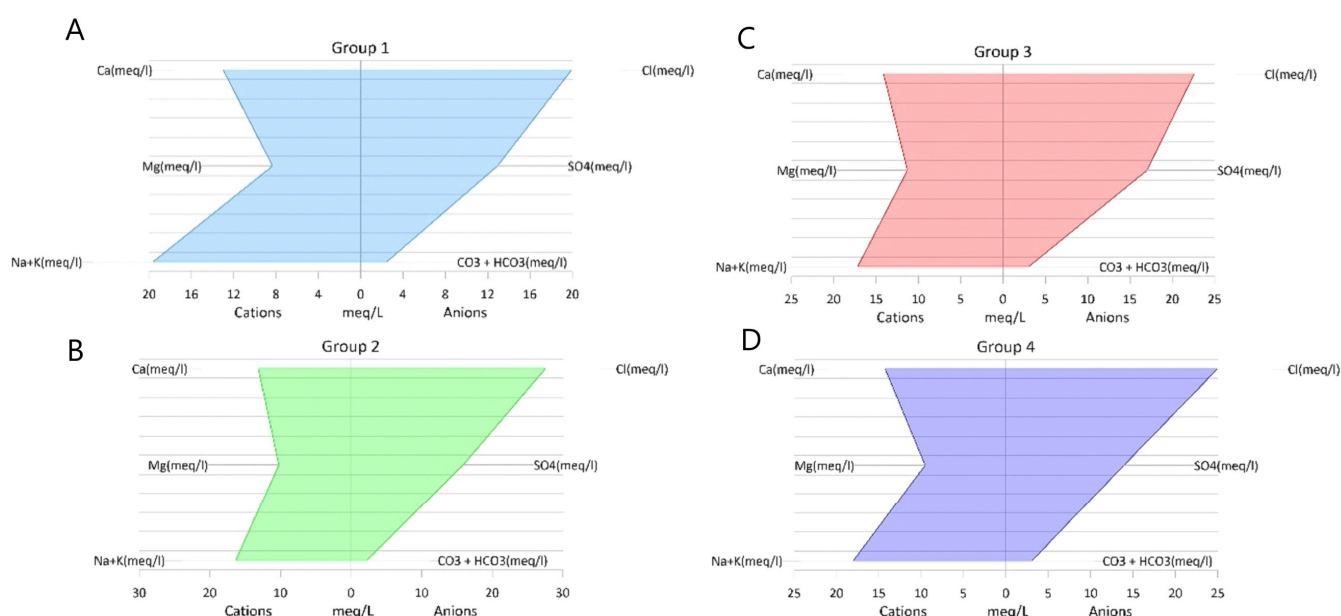
Figure 5. Stiff diagram for the four water groups, (**A**) group 1; (**B**) group 2; (**C**) group 3; (**D**) group 4.
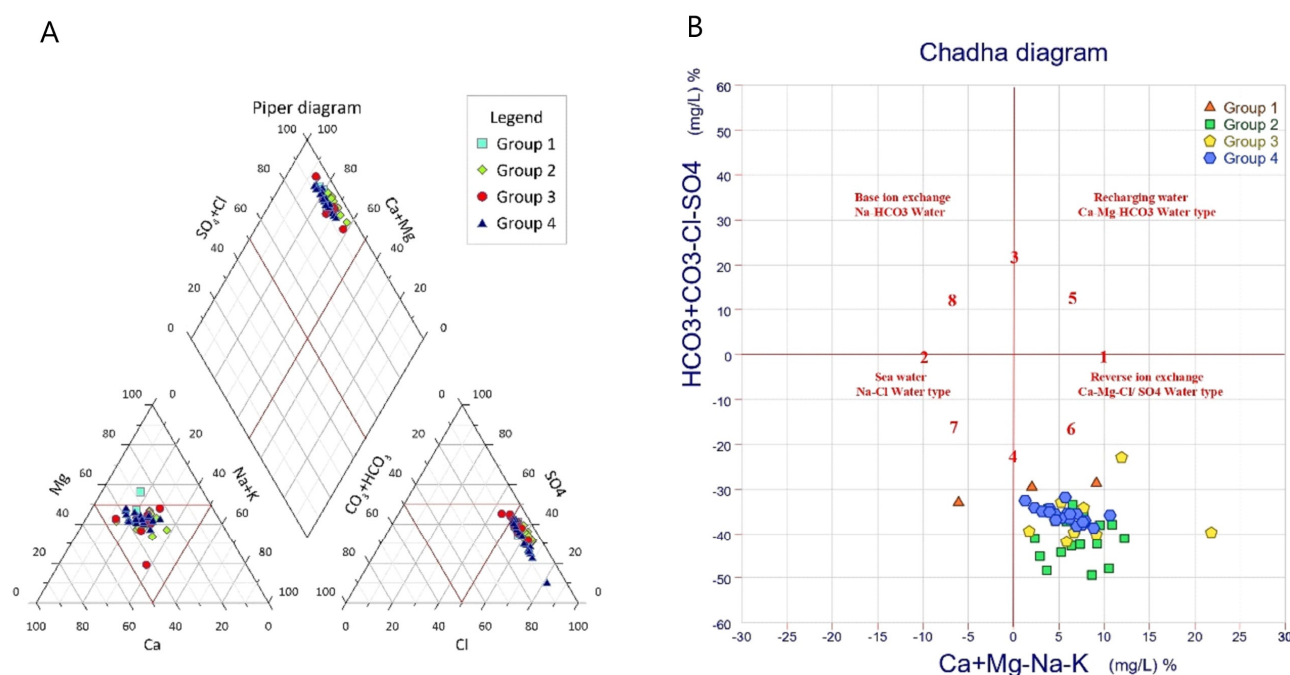
A

B

Figure 6. (**A**) Piper diagram for water samples, and (**B**) Chadha diagram of the groundwater samples.

Group 2 consists of wells (2, 20, 21, 8, 10, 17, 9, 4, 7, 16, 11, 18, 12, 14, 3, 28, and 44). These wells represent 34.69% of the water samples in the study area, where 20.41% of these wells are in El Oued municipality and consist of wells 2, 3, 4, 7, 8, 9, 10, 11, 12, and 14, that belong to the Mio-Pliocene aquifer, and 10.20% of water samples are in Debila (16, 17, 18, 20, and 21), belonging to the Mio-Pliocene aquifer. However, 2.04% of water samples divided between Guemar (W28) and Reguiba (W44) belong to Mio-Pliocene and Pontian, respectively. Extremely high salinity distinguishes this group (3650 < EC < 4430 μS/cm, mean = 4005.44 μS/cm), indicating brackish water. The order of major ions' abundance follows the same order as group 1 (Figure 5), with hydro-chemical facies characterized by Ca-Mg-Cl-SO4 type, CaCl type, and chloride type (Figure 6A). Chloride is simply the most dominant element in this group (min = 815.42 mg/L, max = 1240.86 mg/L, and mean = 976.9 mg/L).In this group Calcium and magnesium were dominated (min = 204.36 mg/L, max = 340.68 mg/L, and mean = 263.24 mg/L for calcium and min = 63.19 mg/L, max = 184.72 mg/L, and mean = 124.26 mg/L for magnesium) values being somewhat lower, while sulphates have been found also high (min = 602.39 mg/L, max = 978.26 mg/L, and mean = 764.12 mg/L). However, chloride, calcium, magnesium, potassium, and sulphates exceeded the desirable WHO 2011 standards for drinking water, while nitrate did not exceed the standards.

Ten wells (1, 15, 19, 25, 27, 30, 31, 41, 47, and 49) constitute group 3, with an average EC of 4272 μS/cm, suggesting brackish water type. W1, 15, 19, and 27 are found in El Oued, Debila, and Guemar, and belong to the Mio-Pliocene aquifer, while 25, 30, 31, 41, 47, and 49 belong to the Pontian aquifer and spread in Guemar, Reguba, and Taghzout. The order of major ions' abundance is $Na^+ + K^+ > Ca^{2+} > Mg^{2+}$ and $SO_4^{2-} > Cl^- > HCO_3^- > NO_3^-$ (Figure 5). Furthermore, the hydro-chemical facies are characterized by Ca-Mg-Cl-SO$_4$ type and CaCl type (Figure 6A). This group is dominated by sulphates and chloride (min = 630.25 mg/L, max = 997.41 mg/L, and mean = 817.62 mg/L) and (min = 457.34 mg/L, max = 985.59 mg/L, and mean = 800.88 mg/L), respectively. Calcium varied from 200.4 to 360.72 mg/L with a mean value of 282.96 mg/L, and magnesium ranged from 63.12 to 165.27 mg/L, with 137.32 mg/L as the mean value. Nitrate had values of min = 16.6 mg/L, max = 28.9 mg/L, and mean = 22.9 mg/L, while potassium and sodium ranged from 32 to 42 mg/L with 36 mg/L as a mean value, and 137 to 460 mg/L with

373.9 mg/L as a mean value, respectively. All the parameters exceeded WHO standards for drinking water except nitrate.

Group 4 consists of nineteen wells (6, 24, 40, 32, 33, 34, 42, 43, 46, 29, 37, 45, 39, 38, 23, 35, 26, 36, and 48), with a mean EC of 4348.95 µs/cm, indicating brackish water: 21.05% of the wells belong to the Mio-Pliocene aquifer (6, 23, 36, and 37) located in El Oued, Guemar, and Kouinine, while 78.95% belong to the Pontian aquifer and are distributed in Guemar, Ourmes, Kouinine, Reguiba, and Taghzout. The concentration of major ions is $Na^+ > Ca^{2+} > Mg^{2+}$ and $Cl^- > SO_4^{2-} > HCO_3^- > NO_3^-$, in that order (Figure 5). The Piper plot also confirmed that hydro-chemical facies are Ca-Mg-Cl-SO_4 type, CaCl type, and chloride type (Figure 6A). This group is dominated by chloride and sulfate (min = 730.33 mg/L, max = 1127.41 mg/L, and mean = 884.46 mg/L) and (min = 193.06 mg/L, max = 923.19 mg/L, and mean = 668.14 mg/L), respectively. Nevertheless, calcium values showed min = 216.43 mg/L, max = 324.65 mg/L, and mean = 283.51 mg/L, while magnesium showed min = 65.62 mg/L, max = 165.27 mg/L, and mean = 117.11 mg/L. Except for nitrate, all of the ions met the WHO 2011 drinking water standards.

The Chadha plot in Figure 6B represents most of the samples (97.96%) in the 6th field (reverse ion-exchange Ca-Mg-Cl/SO_4 water type), revealing Ca-Mg-Cl type, Ca-Mg-dominant Cl type, or Cl^--dominant Ca-Mg type waters (alkaline earth ($Ca^{2+} + Mg^{2+}$) exceed alkali metals ($Na^+ + K^+$) and strong acidic anions ($Cl^- + SO_4^{2-}$) exceed weak acidic anions (HCO_3^-)), confirming the Piper diagram's results. On the other hand, 2.04% are plotted in the 7th field (seawater Na-Cl, which indicates that alkali metals exceed alkaline earth and strong acidic anions exceed weak acidic anions), which is more enhanced in ($Ca^{2+} + Mg^{2+}$) and ($Cl^- + SO_4^{2-}$) than (HCO_3^-).

3.3. Water Quality Index

In this study, the computation of WQI obtained values was compared to the WHO (2011) guidelines. Furthermore, ten parameters have been used in the calculation of the WQI for drinking purposes, EC, pH, Ca^{2+}, Mg^{2+}, Na^+, K^+, Cl^-, SO_4^{2-}, HCO_3^-, and NO_3^-. All wells were classified above 50. Nevertheless, 10.20% of wells had good water quality (11.54% Mio-Pliocene and 8.70% from the Pontian), 24.49% of samples had poor quality (15.38% from Mio-Pliocene and 34.78% from the Pontian), while 55.10% had very poor quality (61.54% of Mio-Pliocene and 47.83% of Pontian). Furthermore, 4.08% are unfit for drinking purposes, including 7.69% of the Mio-Pliocene aquifer (Table 3).

Table 3. WQI-based groundwater suitability for drinking and irrigation.

Range	Classes	Number of Wells	% of Samples (49 Samples)	% of Samples (Mio-Pliocene Sample)	% of Samples (Pontian Sample)
<50	Excellent water	-	-	-	-
100.0–125.0	Good water	W10, W4, W18, W24, W29.	10.20%	11.54%	8.70%
125.1–150.0	Poor water	W13, W21, W11, W28, W44, W30, W47, W40, W26, W38, W39, W48.	24.49%	15.38%	34.78%
150.1–175.0	Very poor water	W5, W22, W2, W20, W8, W17, W7, W16, W12, W14, W19, W15, W25, W27, W49, W41, W31, W6, W32, W33, W34, W42, W46, W23, W35, W36, W37.	55.10%	61.54%	47.83%
175.1–200.0	Unfit for drinking	W9, W3.	4.08%	7.69%	-

The assessment of the collected groundwater samples from the complex terminal aquifer was performed by different indices. The illustration of the results is presented in Table 4. According to the TH (total hardness) values, 44.90% were classified as soft water (53.85% from Mio-Pliocene and 34.78% from the Pontian), and 55.10% are moderately hard

(50% from Mio-Pliocene and 60.87% from Pontian); in contrast, there was no monitoring well observed in the range of hard to very hard, respectively. The SAR values are ranged below class 10, indicating excellent water according to SAR, and it could be utilized for most types of soil. The EC values of the complex terminal aquifer were sorted into two categories: 2.04% (W5) and 4.35% from the Pontian present doubtful water quality, while 97.96% present unsuitable quality for irrigation, and 100% from the Mio-Pliocene and 95.65% from the Pontian. The % Na indicated that 81.63% of the samples are permissible for irrigation (73.08% of Mio-Pliocene and 91.30% from the Pontian), while 18.37% present good quality (26.92% of Mio-Pliocene and 8.70% of Pontian). Meanwhile, one sample was considered as excellent quality. The magnesium hazard index indicates that 85.71% of the samples are suitable for irrigation (80.77% from the Mio-Pliocene and 91.30% from the Pontian); meanwhile, 14.29% of the samples were not suitable for irrigation (19.23% from Mio-Pliocene and 8.70% from the Pontian). The PI presents that 97.96% of the samples are moderate quality, except for W41, which belongs to the Pontian aquifer and is classified as suitable. The Kelley ratio (KR) presents 97.96% of the samples as suitable quality (100% of the Mio-Pliocene and 95.65% of the Pontian), except for W5, which belongs to the Pontian aquifer. According to RSC, 100% of the samples can be acceptable for irrigation practices.

Table 4. Irrigation quality indices of the complex terminal aquifer.

Range	Classes	Number of Wells
EC		
<250	Excellent	
250–750	Good	
750–2000	Permissible	
2000–3000	Doubtful	W5
>3000	Unsuitable	All the samples except W5
(Na%)		
<20	Excellent	W41
20–40	Good	W22, W20, W8, W17, W7, W18, W15, W41, W46.
40–60	Permissible	W5, W13, W2, W21, W10, W9, W4, W16, W11, W12, W14, W3, W28, W44, W1, W19, W25, W27, W49, W30, W47, W31, W6, W24, W32, W33, W34, W40, W42, W43, W23, W26, W29, W35, W36, W37, W38, W39, W45, W48.
60–80	Doubtful	
>80	Unsafe	
SAR		
<10	Excellent	All the samples
10–18	Good	
18–26	Doubtful	
>26	Unsuitable	
TH		
<75	Soft	W36, W13, W2, W10, W4, W16, W11, W12, W14, W3, W28, W19, W6, W36, W38, W39, W29, W35, W40, W24, W30, W5.
75–150	Moderately hard	W22, W20, W21, W8, W17, W9, W7, W18, W1, W15, W27, W23, W37, W44, W25, W49, W41, W47, W31, W33, W34, W42, W43, W46, W26, W45, W48.
150–300	Hard	
>300	Very hard	
MH		
<50	Suitable	W5, W44, W25, W49, W41, W30, W47, W31, W24, W32, W33, W34, W40, W46, W26, W29, W35, W38, W39, W45, W48, W13, W22, W2, W20, W21, W10, W17, W9, W4, W7, W16, W11, W12, W3, W28, W19, W15, W27, W6, W36, W37.
>50	Unsuitable	W1, W8, W14, W18, W42, W43, W23.

Table 4. *Cont.*

	Range	Classes	Number of Wells
	PI		
	<25	Suitable	W41
	25–75	Moderate	All the samples except W41
	>75	Unsuitable	
	KR		
	<1	Suitable	All the samples except W5
	1–2	Moderate	W5
	>2	Unsuitable	
	RSC		
	<1.25	Acceptable	All the samples
	1.25–2.5	Slightly adapted to irrigation	
	>2.5	Not suitable	

3.4. Geostatistical Modeling

The normalcy of the studied water parameters was taken into account, for performing the Kriging interpolation. On the basis of the mean error (ME) and root mean square normalized error (RMSSE) values, the best-fitted semi-variogram models were selected. The model is evaluated based on the precision of the predictions when ME is minimum, and RMSSE is close to unity.

The most important hydro-chemical parameters were fitted to the exponential semi-variogram model, including EC, Ca^{2+}, Mg^{2+}, K^+, Na^+, HCO_3^-, Cl^-, NO_3^-, and SO_4^{2-}. The rational quadratic model was the best-fitting semi-variogram model for Na^+ and NO_3^-. Depending on the nuggets' variance/sill ratio. Moreover, diverse classifications were accustomed to describ the spatial dependence of hydro-chemical groundwater parameters. There were three forms of spatial dependence considered in this study: strong when the ratio is less than 25%, mild when the ratio is between 25% and 75%, and weak when the ratio is greater than 75% (Table 5).

Table 5. Best-fitted semi-variogram models and cross-validation for OK of groundwater quality parameters.

Parameter	Transformation	Semi-Variogram Model Parameters						Prediction Errors	
		Model	Nugget (C_0)	Partial Sill (C)	Sill ($C_0 + C$)	$(\frac{C0}{C0+C}) \times 100(\%)$	Spatial Dependence	Mean	Root-Mean-Square Standardized
EC	Original Data	Exponential	0.0281	0.0976	0.1257	22.35	Strong	0.2280	1.0898
Ca^{2+}	Original Data	Exponential	0.7443	0.6767	1.421	52.37	Moderate	0.8456	0.9513
Mg^{2+}	Logarithmic	Exponential	0.0622	0.0112	0.0734	84.74	Weak	1.0347	0.9107
Na^+	Original Data	Rational Quadratic	0.1121	0.1668	0.2789	40.19	Moderate	−1.8648	1.2353
K^+	Original Data	Exponential	0.1451	0.3571	0.5022	28.89	Moderate	0.2237	1.1311
HCO_3^-	Original Data	Exponential	0.4181	0.5582	0.9763	42.82	Moderate	−0.7022	0.9269
Cl^-	Logarithmic	Exponential	0.02691	0.0048	0.03171	84.864	Weak	−0.5148	0.9050
SO_4^{2-}	Logarithmic	Exponential	0.0070	0.0910	0.098	7.142	Strong	−0.4243	0.7315
NO_3^-	Logarithmic	Rational Quadratic	0.0537	0.3156	0.3693	14.54	Strong	0.9932	1.1166

In the study area, EC, SO_4^{2-}, and NO_3^- have a strong structure of spatial dependance, while Ca^{2+}, Na^+, K^+, and HCO_3^- have a moderate spatial structure. Mg^{2+} and Cl^- both have a weak spatial structure of spatial dependance.

The spatial distribution of the EC (Figure 7) shows that the mineralization increases from the east of the study area towards the west and southwest part as a result of the local geology of the region in addition to the serious situation of some wells of the complex terminal, which present perforations in the level of casings, which favor the communication and the contact between the phreatic aquifer, which is also characterized by high mineralization.
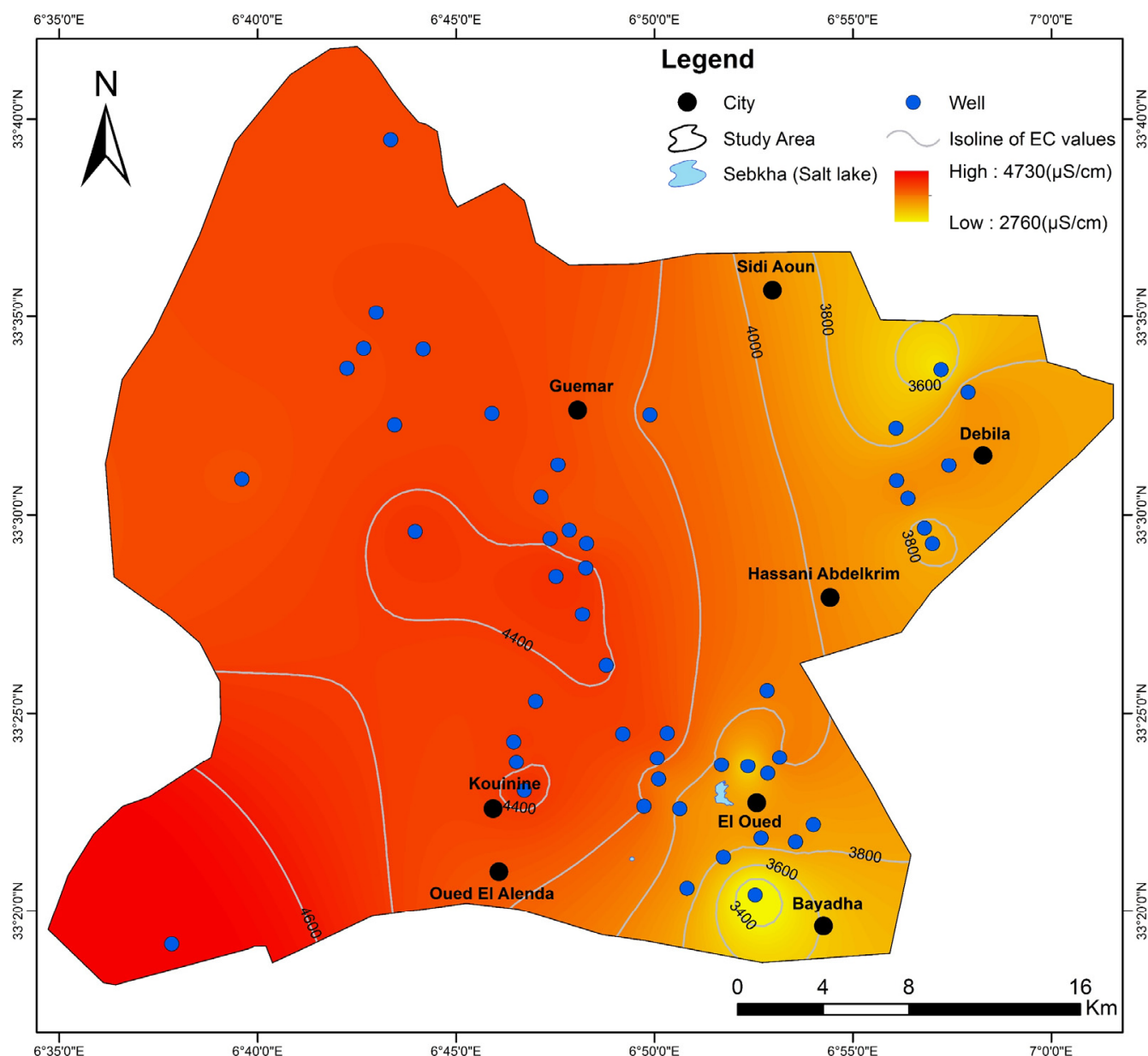
Figure 7. Spatial distribution of EC.

The dissolution of evaporate formations, the leaching of clays, and the dissolution of gypsum and anhydrite are the main factors that control the spatial distribution of SO_4^{2-} and Mg^{2+}. Low values were found in the north of the study area around Sidi Aoun and Guemar, while the highest values were observed in the southwest of the study area. The lowest values of Mg^{2+} were located near Guemar, southwest of Debila, south of El Oued, and Kouinine. Furthermore, a high value was also noted in the southwest, as shown in Figures 8B and 9C.
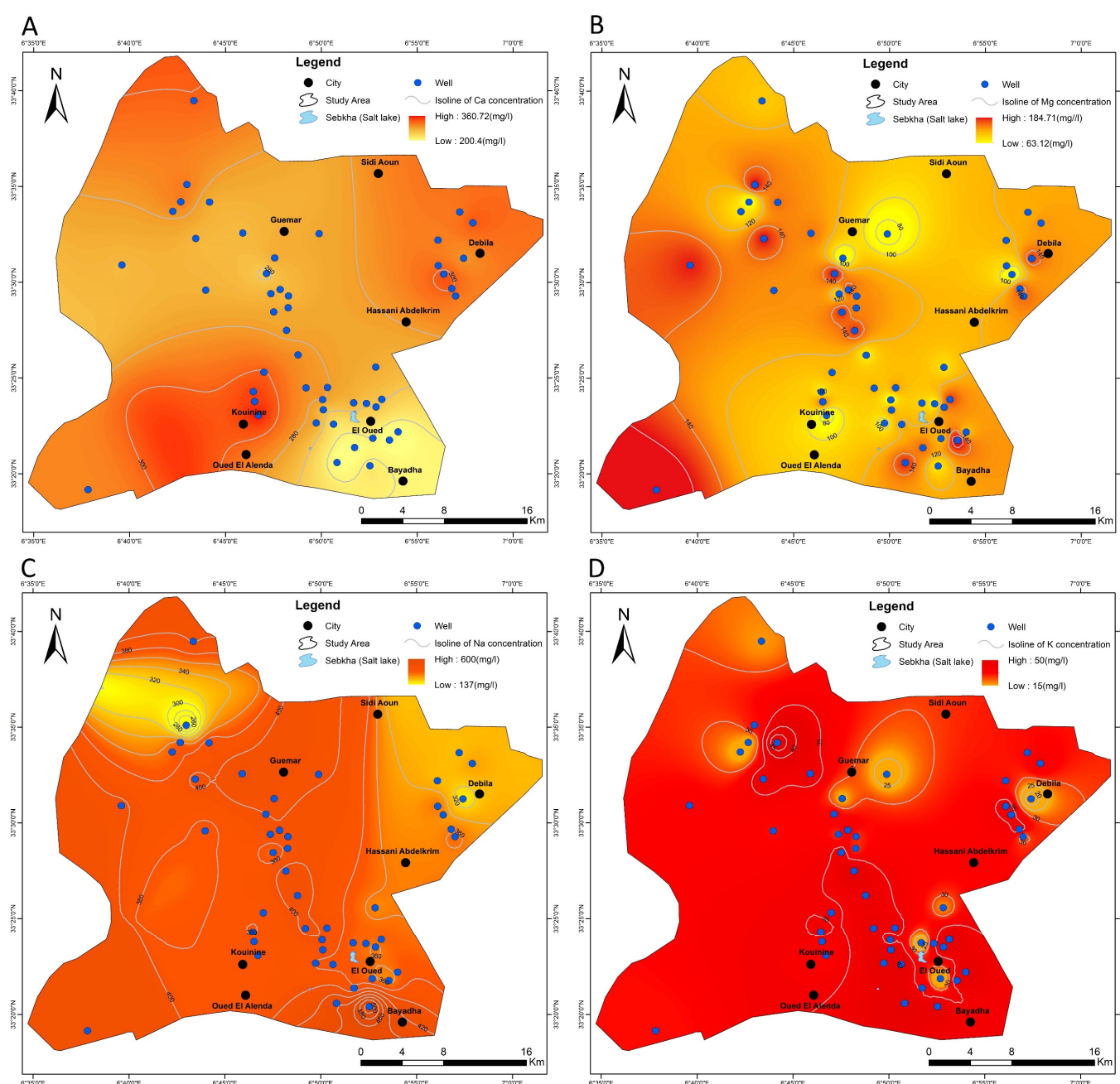
Figure 8. Spatial distribution of cations: (**A**) calcium, (**B**) magnesium, (**C**) sodium, (**D**) potassium.

The spatial distribution maps for Ca^{2+}, HCO_3^-, Na^+, K^+, and Cl^- show a high heterogeneity due to the high geological variation areas as well as the depth of each well. Ca^{2+} concentrations are low to the south of El Oued, while the high values were found in Debila, Sidi Aoun, and Kouinine. Ca increased in the south of the study area (Kouinine) and in the northwest and around Debila and Sidi Aoun. At the same time, it was decreased from Guemar towards El Oued, until Bayadha. Additionally, HCO_3^- increased from El Oued (southeast) to the northwest and southwest, as shown in Figures 8A and 9B.

The existence of sodium is linked, in essence, to the dissolution of halite (evaporates). Indeed, sodium, as for chlorides, displays high and non-homogeneous contents in the waters of the complex terminal (CT). The sodium levels in the CT groundwater samples decreased in the northeast of the study area, near Debila, and in the northwest. Figures 8C and 9A show that the chloride concentration increases from the west to the east.
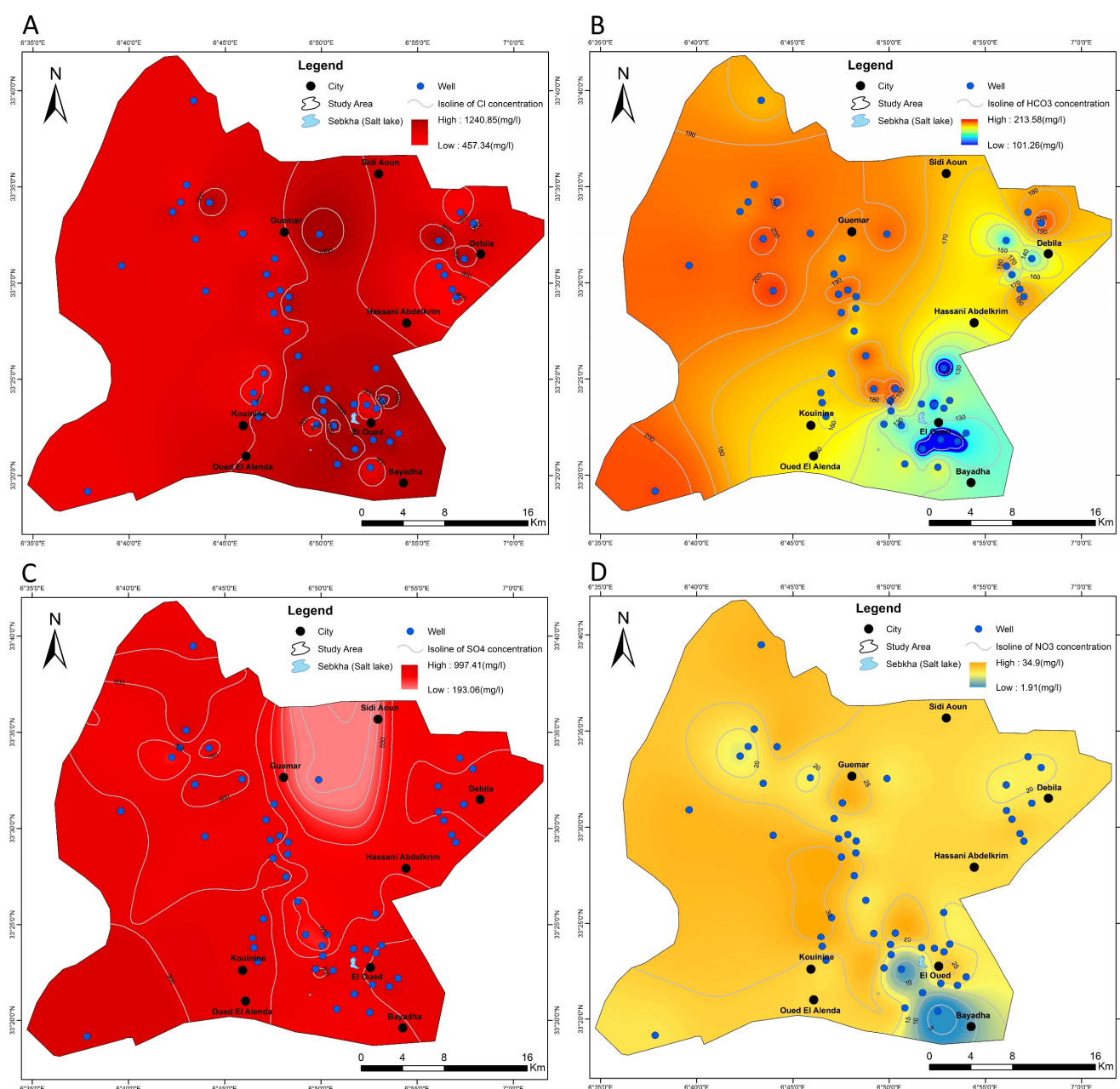
Figure 9. Spatial distribution of anions: (**A**) Cl^-, (**B**) HCO_3^-, (**C**) SO_4^{2-}, (**D**) NO_3^-.

Potassium comes mainly from evaporites, in this case, sylvite (KCl), or as a result of an alteration of potassium clays in the phreatic and complex terminal aquifer. The study area is characterized by high values of potassium, except for some zones where the potassium concentrations are very low, such as Debila, Guemar, and El Oued, as shown in Figure 8D.

Nitrate mainly comes from the contamination of wastewater in urban areas and fertilizers in agricultural lands. Figure 9D reveals that the high values of nitrates are found in the northwest and west of the study area, north of Guemar, north of Kouinine, and east and north of El Oued. The high values of nitrates confirm the dilution between the phreatic groundwaters and the complex terminal flows, resulting in considerable amounts of nitrates in the complex terminal waters. The low values are registered in the ghouts covered with reeds because of their use for the growth of reeds and at the level of the release of El Oued, where the oxygen necessary for the respiration of microorganisms is provided by the denitrification of nitrates.

3.5. Origin of Mineralization

Lithology influences groundwater mineralization in arid and semi-arid environments [71]. However, carbonate dissolution, evaporite dissolution, and silicate weathering are three major processes that contribute to the generation of solutes in groundwater systems [41]. The weathering concentrations of evaporites and carbonates, on the other hand, are up to 80 and 12 times faster than those of silicates, respectively. Consequently, even small amounts of carbonates and evaporites might have a big impact on water chemistry [72]. Figure 10A reveals that the dissolution of calcite is the main reaction in 40.81% of groundwater samples, with a ratio of 1 and 2, although 59.18% of samples have a ratio greater than 2, suggesting a non-carbonated mineral source that could play a role in groundwater chemistry, most likely due to reverse cation exchange caused by clay adsorption of calcium and magnesium in the groundwater and/or gypsum dissolution [73]. Due to the pH variation, carbonates (calcite and dolomite) dissolve mostly in the form of HCO_3^-.
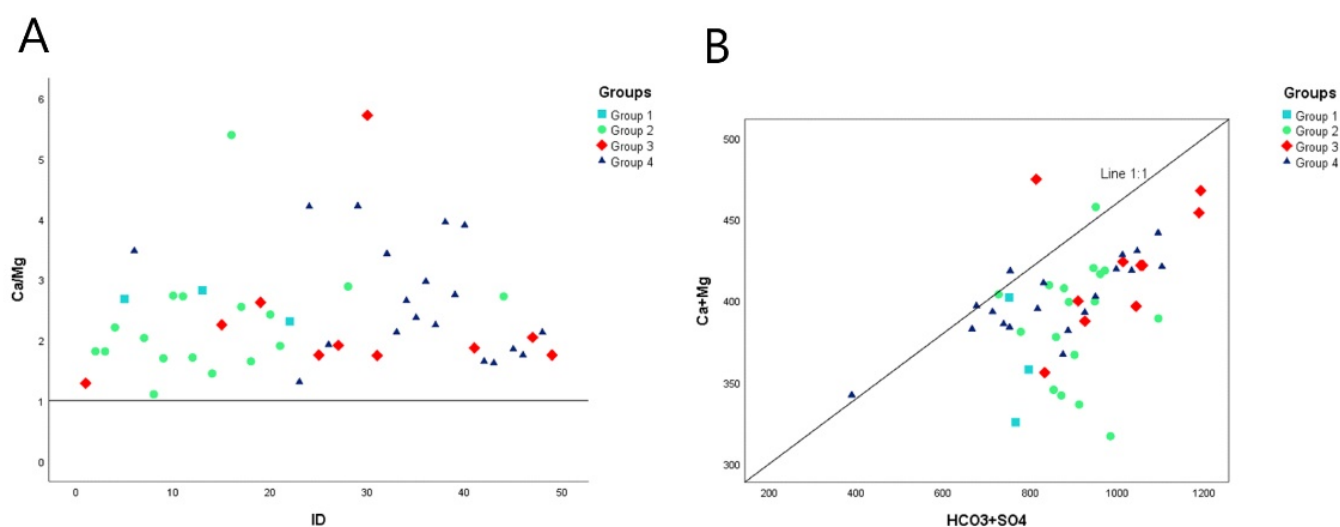

Figure 10. (**A**) Bivariate plots of a good number vs. Ca^{2+}/Mg^{2+}, and (**B**) bivariate plots of $Ca^{2+} + Mg^{2+}$ vs. $HCO_3^- + SO_4^{2-}$.

The majority of the points in Figure 10B are plotted on the right side, indicating that ion exchange dominates reverse ion exchange due to an excess of $(SO_4^{2-} + HCO_3^-)$. However, line 1:1 is very close to 47.37% of group 4 samples and 17.65% of group 2 samples, demonstrating that calcite, dolomite, anhydrite, and gypsum would be the primary reactions in the system for the concerned group. Group 1 has only one sample that is close to line 1:1 [74–76].

In Figure 11A [77], a Na^+-normalized Ca^{2+} vs. HCO_3^- graph shows that the four group samples vary in their sensitivity to silicate weathering. The Na^+-normalized vs. Mg^{2+} plot in Figure 11B indicates that the four group samples range from being affected by silicate weathering with a weak tendency, to evaporates' dissolution.

3.6. Controlling Mechanisms

Gibbs's diagrams signifying the variation of $[Cl^-/(Cl^-/HCO_3^-)]$ and $[Na^+/(Na^+/Ca^{2+})]$ ratios as a function of TDS. Precipitation, rock, and evaporation dominance are illustrations of these diagrams that are widely used to determine the structural origins of dissolved chemical components. Figure 12 shows the Gibbs plots of cation and anion ratios against TDS for each of the four groups. Chemical data from all the clustered groups are plotted in the evaporation–precipitation dominance part, suggesting that evaporation–precipitation has a strong influence on water quality.
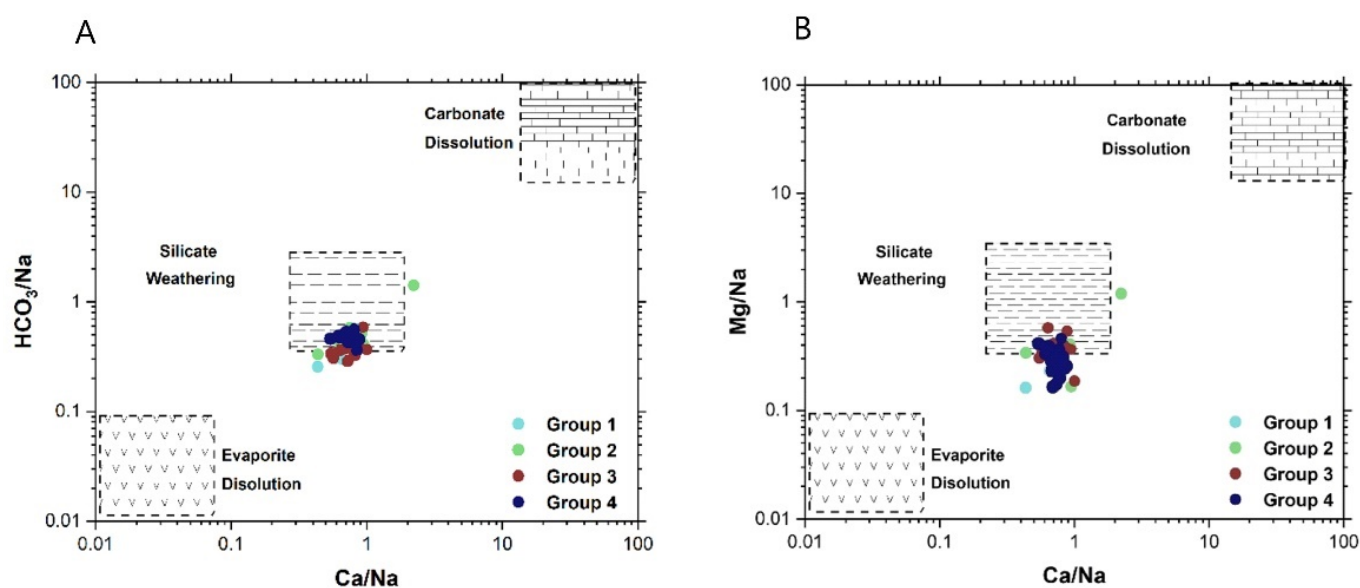
Figure 11. (**A**) Molar ratio in bivariate plots of Na^+-normalized Ca^{2+} and HCO_3^-, and (**B**) Na^+-normalized Ca^{2+} and Mg^{2+}.
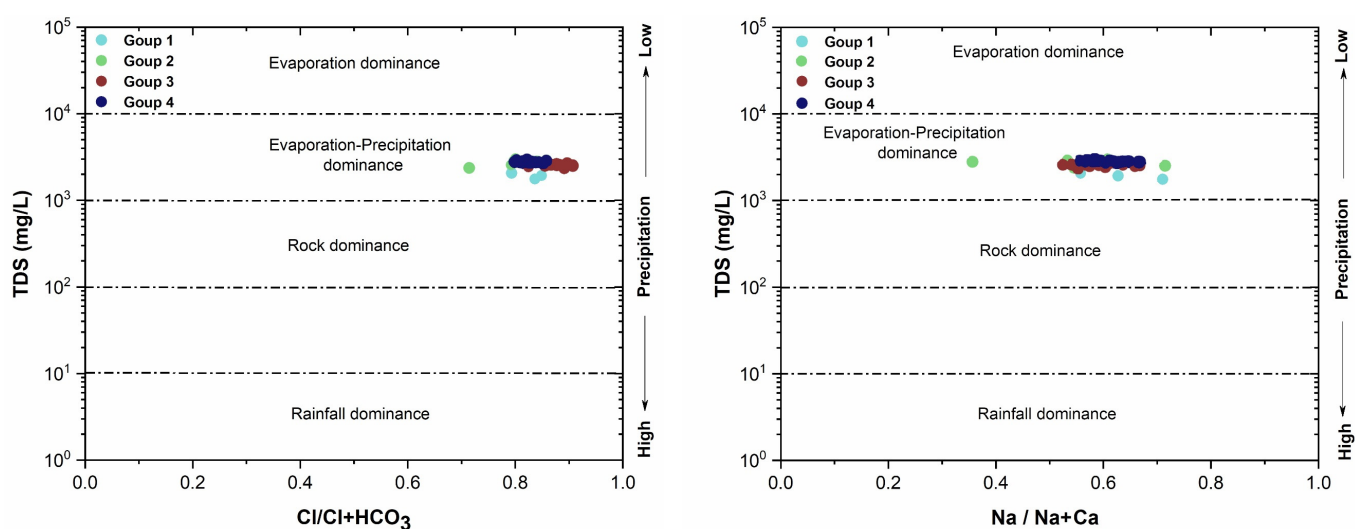

Figure 12. Gibbs diagrams of the complex terminal groundwater aquifer.

For the assessment of ion exchange reactions between groundwater and its host rock [69,78], the chloro-alkaline indices (CAI) are widely used by suggesting two chloro-alkaline indices (CAI I, II) for the interpretation of ion exchange between groundwater and host environment.

The exchange of Na^+ and K^+ from the water with Mg^{2+} and Ca^{2+} of the rocks is shown by the positivity of chloro-alkaline indices (base-exchange reaction). Meanwhile, negative chloro-alkaline indices mean that Mg^{2+} and Ca^{2+} from the water are exchanged with Na^+ and K^+ of the rocks. Figure 13 shows that most of the complex terminal groundwater aquifers have positive chloro-alkaline indices, explained by the substitution of Ca^{2+} and Mg^{2+} in groundwater with Na^+ and K^+ in the aquifer system.
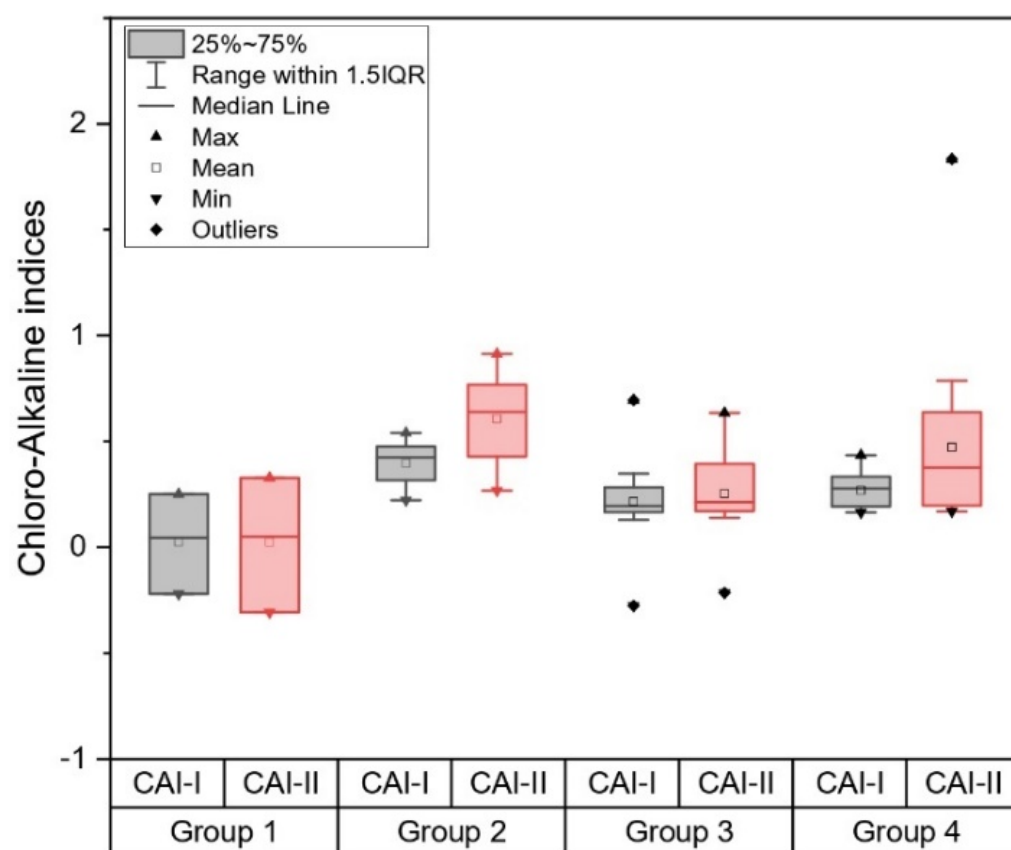
Figure 13. Chloro-alkaline indices for the four groups.

3.7. Geochemical Modeling

Positive saturation index values suggest oversaturation and a tendency for the mineral to precipitate from the groundwater. Negative values all at once suggest undersaturation and, as a result, mineral dissolution into groundwater. The equilibrium condition occurs when the saturation index is between -0.5 and $+0.5$, and it indicates that the mineral in this groundwater is not dissolving or precipitating [79]. The dissolution of anhydrite, gypsum, and halite is identified in group 1, while aragonite, calcite, dolomite, and sylvite all have a supersaturation state. Aragonite, calcite, and dolomite are supersaturated in group 2 (precipitated). Anhydrite, gypsum, halite, and sylvite, on the other hand, are dissolved.

Aragonite, calcite, and dolomite were found to precipitate in group 3. Anhydrite, gypsum, halite, and sylvite were all dissolved during the process. In group 4, almost the same minerals are precipitating and dissolving. Figure 14 shows that evaporated minerals (anhydrite, gypsum, and halite) are undersaturated in most of the groups due to the dry environment and low precipitation in the study area, which leads to high evaporation in the surface water, making the uppermost aquifer (the phreatic aquifer) very mineralized compared to the complex terminal aquifer. The fact that evaporated minerals in groundwater samples are undersaturated shows that their soluble elements Na^+, Cl^-, Ca^{2+}, and SO_4^{2-} are not constrained by mineral equilibrium. Table 6 shows the outcomes from several minerals' saturation indices' computations (anhydrite, aragonite, calcite, dolomite, gypsum, halite, and sylvite).
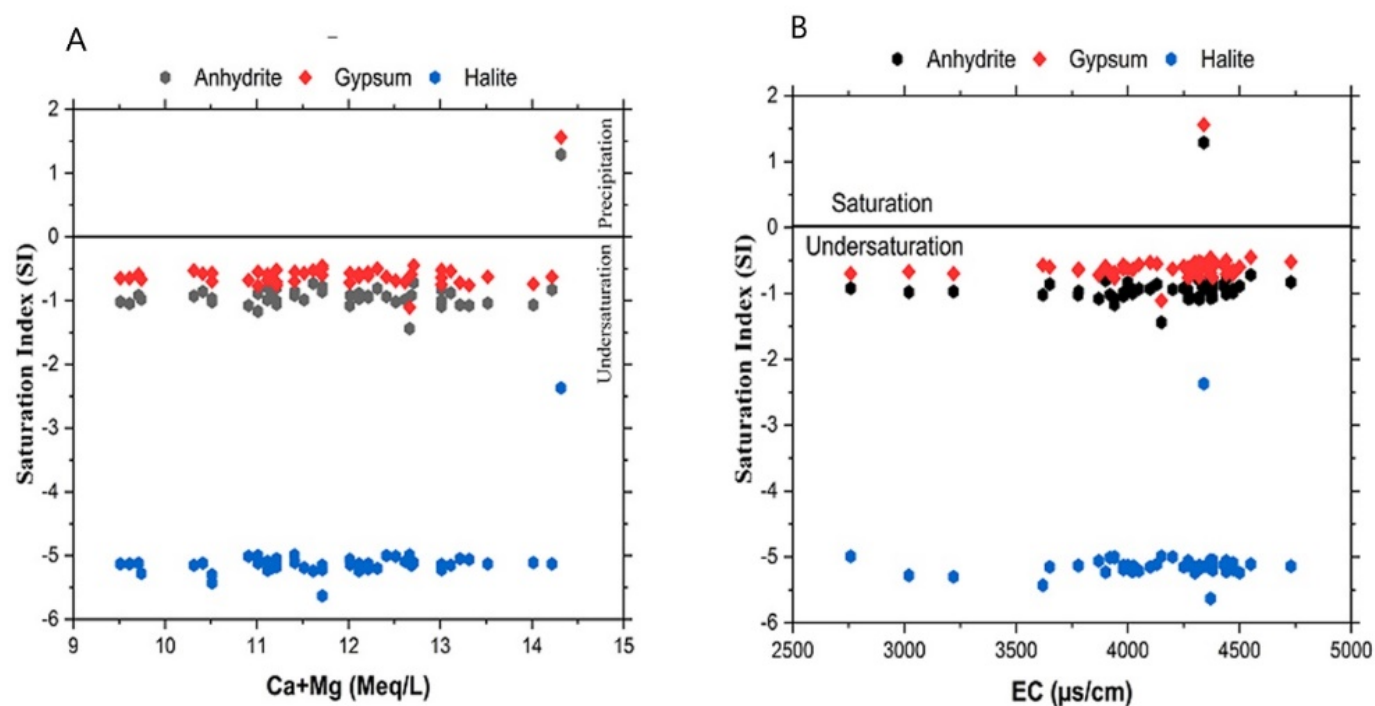
Figure 14. (**A**,**B**) Saturation indices of evaporate minerals.

Table 6. Saturation indices of minerals in groundwater with statistical summary using PHREEQC.

Groups	Minerals	Total (Wells)	Mean	SD	Min	Max
Group 1	Anhydrite	3	−0.95667	0.03215	−0.98	−0.92
	Aragonite	3	0.40333	0.34675	0.12	0.79
	Calcite	3	0.54333	0.34429	0.27	0.93
	Dolomite	3	1.04333	0.74895	0.41	1.87
	Gypsum	3	−0.69	0.01732	−0.7	−0.67
	Halite	3	−5.19	0.17349	−5.3	−4.99
	Sylvite	3	−5.84667	0.05859	−5.89	−5.78
Group 2	Anhydrite	17	−0.95588	0.08718	−1.08	−0.8
	Aragonite	17	0.18471	0.17288	−0.17	0.46
	Calcite	17	0.33235	0.16995	−0.02	0.59
	Dolomite	17	0.62647	0.37959	−0.05	1.28
	Gypsum	17	−0.62118	0.05243	−0.72	−0.53
	Halite	17	−5.12118	0.06855	−5.23	−5
	Sylvite	16	−5.75688	0.18062	−6.08	−5.51
Group 3	Anhydrite	10	−0.918	0.12541	−1.17	−0.72
	Aragonite	10	0.261	0.14798	0.05	0.49
	Calcite	10	0.409	0.14617	0.19	0.64
	Dolomite	10	0.779	0.36765	0.3	1.29
	Gypsum	10	−0.575	0.09192	−0.77	−0.45
	Halite	10	−5.208	0.1839	−5.63	−5
	Sylvite	10	−5.763	0.08957	−5.91	−5.57
Group 4	Anhydrite	19	−0.85263	0.54216	−1.44	1.29
	Aragonite	19	0.47579	0.56655	0.2	2.78
	Calcite	19	0.62	0.56805	0.34	2.93
	Dolomite	19	1.15684	1.04431	0.47	5.37
	Gypsum	19	−0.54368	0.52915	−1.11	1.56
	Halite	19	−4.98105	0.63605	−5.24	−2.37
	Sylvite	19	−5.62211	0.6585	−5.91	−2.93

4. Conclusions

The techniques included in this study (hierarchical clustering analysis, geostatistical modeling, and the *WQI*) assisted in the identification of the factors that influence groundwater chemistry in the study area (Oued souf valley—southeast of Algeria).

A review of clustering based on groundwater quality datasets, using Q-mode (Ward's linkage method with the Euclidean distance), defined four major water types. In terms of electrical conductivity, all the groups reflected high to brackish water, with mean values of 3000, 4005.44, 4272, and 4348.95 µS/cm, respectively. At the same time, all the groups had the same hydro-chemical facies of Ca-Mg-Cl-SO$_4$. In the first and second groups, however, chloride was the dominant ion (mean = 706.7 mg/L and 815.42 mg/L, respectively). Groups 3 and 4 were dominated by chloride and sulphates (mean = 817.62 mg/L for chloride and 800.88 mg/L for sulphates in group 3, where means for chloride and sulphate were 884.46 mg/L and 668.14 mg/L respectively in group 4).

Ordinary Kriging geostatistical analysis revealed a strong spatial structure for EC, SO$_4{}^{2-}$, and NO$_3{}^-$ and a moderate spatial structure for Ca^{2+}, Na$^+$, K$^+$, and HCO$_3{}^-$. Furthermore, Mg^{2+} and Cl$^-$ have weak spatial structures. Owing to the high geological variation of the study area and the depth of each well, the spatial distribution maps for Ca^{2+}, HCO$_3{}^-$, Na$^+$, K$^+$, and Cl$^-$ revealed high heterogeneity. El Oued to the south had low Ca^{+2} concentrations, while Debila, Sidi Aoun, and Kouinine had higher Ca^{2+} concentrations.

The complex terminal groundwater's WQI values indicated unfitness for drinking uses. However, the irrigation indices showed that these groundwaters are of excellent to moderate irrigation quality. The dissolution of calcite controls 40.81% of groundwater samples, even though 59.18% of samples had a non-carbonate mineral origin, which may play a role in groundwater chemistry due to reverse cation exchange caused by clay adsorption and/or gypsum dissolution. Due to an excess of (SO$_4{}^{2-}$ + HCO$_3{}^-$), ion exchange was expected to dominate over reverse ion exchange. However, 47.37% of group 4 and 17.65% of group 2 samples showed the dominant reactions in the CT groundwater system. The geochemical evolution of the groundwater samples indicates an undersaturation of evaporated minerals in the study area, in contrast, the precipitation of the carbonate minerals has been occurred.

The study's key conclusion is that the agricultural and economic growth of the Oued souf region has directly resulted in overexploitation of deep groundwater aquifers, mainly the complex terminal aquifer, which has a long-term impact on their quantitative and qualitative aspects, particularly in some vulnerable areas.

References

1. Ravikumar, P.; Somashekar, R.K.; Angami, M. Hydrochemistry and evaluation of groundwater suitability for irrigation and drinking purposes in the Markandeya River basin, Belgaum District, Karnataka State, India. *Environ. Monit. Assess.* **2011**, *173*, 459–487. [CrossRef]
2. OSS. *Système Aquifère du Sahara Septentrional: Modèle Mathématique*; Observatoire du Sahara et du Sahel—Sahara and Sahel Observatory: Tunis, Tunisia, 2003.
3. Harrat, N.; Achour, S. Pollution physico-chimique des eaux de barrage de la region d' el tarf. impact sur la chloration. *Larhyss J.* **2010**, *8*, 47–54.
4. ANRH. *Ressources en Eau et en Sols de l'Algérie*; Rapport Technique; ANRH: Alger, Algeria, 1986.
5. CDTN. *Etude Hydrochimique et Isotopique des Eaux Souterraines de la Cuvette de Ouargla*; Rapport Technique; CDTN: Alger, Algeria, 1992.
6. Miloudi, A.M.; Remini, B. Water Potentiality of Sustainable Management Challenges in the Oued Souf Region, south east Algeria. *Int. J. Energetica* **2016**, *1*, 36–39. [CrossRef]
7. Bel, F.; Demargne, F. *Etude Géologique du Continental Terminal*; Rapport Technique; ANRH: Alger, Algeria, 1966; Volume 24, p. 22.
8. Busson, G. *Principes, Methodes et Resultats d'une Etude Stratigraphique du Mesozoique Saha-Rien*; BRGM: Paris, France, 1972; Volume 26, p. 441.
9. Fabre, F. *Introduction A la Géologie du Sahara d'Algérie et des Régions Voisines*; SNED: Algiers, Algeria, 1976; p. 442.
10. Cornet, A. Introduction à l'hydrogéologie Saharienne. *Géorg. Phys. Géol. Dyn.* **1964**, *61*, 5–72.
11. Bel, F.; Cuche, D. *Etude des Nappes du Complexe Terminal du Bas Sahara*; Données Géologiques et Hydrogéologiques Pour la Construction du Modèle Mathématique; Rapport Technique; DHW: Ouargla, Algeria, 1970.
12. Castany, G. Bassin Sédimentaire du Sahara Septentrional (Algérie Tunisie). Aquifères du Continental Intercalaire et du Complexe Terminal. *Bull. Bur. Rec. Géol. Min.* **1982**, *3*, 127–147.
13. Halassa, Y.; Zeddouri, A.; Mouhamadou, O.B.; Kechiched, R.; Benhamida, A.S. Hydrogeological study of the aquifer system of the northern Sahara in the Algero-Tunisian border: A case study of Oued Souf region. *AIP Conf. Proc.* **2018**, *1968*, 030010. [CrossRef]
14. Tabouche, N.; Achour, S. Etude de la Qualité des Eaux Souterraines de la Région Orientale du Sahara Septentrional Algérien. *Larhyss J.* **2010**, *3*, 99–113.
15. Chebbah, M.; Allia, Z. Geochemistry and hydrogeochemical process of groundwater in the Souf valley of Low Septentrional Sahara, Algeria. *Afr. J. Environ. Sci. Technol.* **2015**, *9*, 261–273. [CrossRef]
16. Habes, S.; Djabri, L.; Bettahar, A. Water quality in an arid weather area, case: Ground water of terminal complex and con-tinental intercalary, algerian southeast. *Larhyss J.* **2016**, *28*, 55–63.
17. Megdoud, M. (ANRH, Paris, France). Personal communication, 2003.
18. Djellouli, H.; Taleb, M.; Harrache, S.C.D.D. Qualité Physico-Chimique des Eaux de Boisson du sud Algérien: Étude de l'excès En Sels Minéraux. *Cah. Santé.* **2005**, *15*, 109–112.
19. Zaiz, I.; Zine, B.; Boutoutaou, D.; Khechana, S. Contribution to the study of the quality physicochemical of the waters of the water of the complex terminal in the valley of Oued Souf (South-East Algerian). *J. Fundam. Appl. Sci.* **2017**, *9*, 1559. [CrossRef]
20. Moulla, A.S.; Guendouz, A. *Etude des Ressources en eau Souterraine en Zones Arides (Sahara Algerien) par les Methodes Isotopiques*; IAHS Publication: Wallingford, UK, 2003.
21. Slimani, R.; Guendouz, A.; Trolard, F.; Moulla, A.S.; Hamdi-Aïssa, B.; Bourrié, G. Identification of dominant hydrogeochemical processes for groundwaters in the Algerian Sahara supported by inverse modeling of chemical and isotopic data. *Hydrol. Earth Syst. Sci.* **2017**, *21*, 1669–1691. [CrossRef]
22. Khechana, S.; Derradji, E. Qualité Des Eaux Destinées à La Consommation Humaine et à l' Utilisation Agricole (Cas Des Eaux Souterraines d' Oued-Souf, SE Algérien), Maroc Tunisie. *Synth. Rev. Sci. Technol.* **2014**, *28*, 58–68.
23. Khebizi, H.; Benlaoukli, B.; Bouaicha, F.; Adadzi, P.; Bouras, O. Salinization Origin of Souf Terminal Complex: Application of Statistical Modelling and WQI for Groundwater Management. *Hydrol. Earth Syst. Sci. Discuss.* **2020**, 1–16. [CrossRef]
24. Mameri, N.; Yeddou, A.R.; Lounici, H.; Belhocine, D.; Grib, H.; Bariou, B. Defluoridation of septentrional Sahara water of north Africa by electrocoagulation process using bipolar aluminium electrodes. *Water Res.* **1998**, *32*, 1604–1612. [CrossRef]
25. Achour, S.; Youcef, L. Excès des Fluorures Dans les Eaux du Sahara Septentrional Oriental et Possibilité de Traitement. *EIN Int.* **2001**, *6*, 47–54.
26. Ramdani, A.; Taleb, S.; Mebarka, D.H. Seasonal Changes Comparison of Physico-Chemical and Bacteriological Characteris-tics of Water in Some Regions of Southern Algeria. *Phytochem. BioSub J.* **2016**, *10*, 21–32.
27. Abdaoui, G.R.; Tabet, A.A.; Bouaicha, F.; Bousmaha, A.; Bouchemal, S. Sprawl, Specificity and Dynamics of Inter-Municipal Urban Agglomerations of the Souf Valley (South East Algeria): Using GIS Techniques. *Int. J. Innov. Appl. Stud.* **2020**, *29*, 991–1014.
28. Remini, B.; Souaci, B.E. Le Souf: Quand le forage et le pivot menacent le Ghout. *Larhyss J.* **2019**, *37*, 23–38.
29. Bataillon, C. *Le Souf. Etude de Géographie Humaine. Mémoire No 2, Universite d'Alger*; Institut de Recherches Sahariennes: Algiers, Algeria, 1955.
30. Kadri, S.R.; Chaouche, S. La remontée des eaux dans la région du Souf: Une menace sur un écosystème oasien. *Les Cah. d'EMAM* **2018**, *30*. [CrossRef]

31. Remini, B.; Kechad, R. Impact of the Water Table Razing on the Degradation of el Oued Palm Plantation (Algeria) Mechanisms and Solutions. *Int. J. Geogr. Tech.* **2011**, *1*, 48–56.

32. Dubief, J. Persée-Portail des Revues Scientifiques en SHS. *Ann. Geogr.* **1959**, *74*, 360–361.

33. Giraud, R. Le Continental Terminal en Algérie. Giraud R. le Cont. Termin. en Algérie. *Ann. Fac. Sci. Dakkar* **1978**, *31*, 85–87.

34. Nesson, C. *L'Evolution des Ressources Hydrauliques Dans les Oasis du Bas Sahara Algérien. Recherche sur l'Algérie*; Mémoire et Documents; CNRS: Paris, France, 1975; pp. 7–99.

35. Dervieux, F. La Nappe Phréatique du Souf (Région d'El Oued, Algérie)-Etude du Renouvellement de La Nappe. *Terres et eaux OCRS 3trim* **1957**, *56*, 12–39.

36. Rodier, J.; Legube, B.M. *Analysis of Water, Natural Water, Waste Water, Sea Water; Chemistry, Physical Chemistry*; Bacteriology and Biology: Paris, France, 1984.

37. Bhuiyan, M.A.H.; Suruvi, N.I.; Dampare, S.B.; Islam, M.A.; Quraishi, S.B.; Ganyaglo, S.; Suzuki, S. Investigation of the possible sources of heavy metal contamination in lagoon and canal water in the tannery industrial area in Dhaka, Bangladesh. *Environ. Monit. Assess.* **2010**, *175*, 633–649. [CrossRef]

38. Foued, B.; Hénia, D.; Lazhar, B.; Nabil, M.; Nabil, C. Hydrogeochemistry and geothermometry of thermal springs from the Guelma region, Algeria. *J. Geol. Soc. India* **2017**, *90*, 226–232. [CrossRef]

39. Güler, C.; Kurt, M.A.; Alpaslan, M.; Akbulut, C. Assessment of the impact of anthropogenic activities on the groundwater hydrology and chemistry in Tarsus coastal plain (Mersin, SE Turkey) using fuzzy clustering, multivariate statistics and GIS techniques. *J. Hydrol.* **2012**, *414–415*, 435–451. [CrossRef]

40. Environ, J. A Multivariate Statistical Analysis of Groundwater Chemistry Data. *Int. J. Environ. Res. (IJER)* **2011**, *5*, 537–544.

41. Belkhiri, L.; Boudoukha, A.; Mouni, L.; Baouz, T. Multivariate Statistical Characterization of Groundwater Quality in Ain Azel Plain, Algeria. *Afr. J. Environ. Sci. Technol.* **2010**, *4*, 526–534.

42. Bouteraa, O.; Mebarki, A.; Bouaicha, F.; Nouaceur, Z.; Laignel, B. Groundwater quality assessment using multivariate analysis, geostatistical modeling, and water quality index (WQI): A case of study in the Boumerzoug-El Khroub valley of Northeast Algeria. *Acta Geochim.* **2019**, *38*, 796–814. [CrossRef]

43. Bouaicha, F.; Dib, H.; Bouteraa, O.; Manchar, N.; Boufaa, K.; Chabour, N.; Demdoum, A. Geochemical assessment, mixing behavior and environmental impact of thermal waters in the Guelma geothermal system, Algeria. *Acta Geochim.* **2019**, *38*, 683–702. [CrossRef]

44. Piper, A.M. A graphic procedure in the geochemical interpretation of water-analyses. *Trans. Am. Geophys. Union* **1944**, *25*, 914–928. [CrossRef]

45. Chadha, D.K. A proposed new diagram for geochemical classification of natural waters and interpretation of chemical data. *Hydrogeol. J.* **1999**, *7*, 431–439. [CrossRef]

46. Gibbs, R.J. Mechanisms Controlling World Water Chemistry. *Science* **1970**, *170*, 1088–1090. [CrossRef]

47. Chen, L.; Feng, Q. Geostatistical analysis of temporal and spatial variations in groundwater levels and quality in the Minqin oasis, Northwest China. *Environ. Earth Sci.* **2013**, *70*, 1367–1378. [CrossRef]

48. Montero, J.; Fernández-Avilés, G.; Mateu, J. *Spatial and Spatio-Temporal Geostatistical Modeling and Kriging*; Wiley: New York, NY, USA, 2015.

49. Kumar, A.; Maroju, S.; Bhat, A. Application of ArcGIS geostatistical analyst for interpolating environmental data from observations. *Environ. Prog.* **2007**, *26*, 220–225. [CrossRef]

50. Webster, R.; Oliver, M.A. *Geostatistics for Environmental Scientists*, 2nd ed.; John Wiley & Sons Ltd.: Chichester, UK, 2007; ISBN 9780470028582.

51. Seo, Y.; Kim, S.; Singh, V.P. Estimating Spatial Precipitation Using Regression Kriging and Artificial Neural Network Residual Kriging (RKNNRK) Hybrid Approach. *Water Resour. Manag.* **2015**, *29*, 2189–2204. [CrossRef]

52. Seyedmohammadi, J.; Esmaeelnejad, L.; Shabanpour, M. Spatial variation modelling of groundwater electrical conductivity using geostatistics and GIS. *Model. Earth Syst. Environ.* **2016**, *2*, 1–10. [CrossRef]

53. Mei, K.; Liao, L.; Zhu, Y.; Lu, P.; Wang, Z.; Dahlgren, R.A.; Zhang, M. Evaluation of spatial-temporal variations and trends in surface water quality across a rural-suburban-urban interface. *Environ. Sci. Pollut. Res.* **2014**, *21*, 8036–8051. [CrossRef]

54. Venkatramanan, S.; Chung, S.Y.; Kim, T.H.; Kim, B.-W.; Selvam, S. Geostatistical techniques to evaluate groundwater contamination and its sources in Miryang City, Korea. *Environ. Earth Sci.* **2016**, *75*, 994. [CrossRef]

55. Adhikary, P.P.; Chandrasekharan, H.; Chakraborty, D.; Kamble, K. Assessment of groundwater pollution in West Delhi, India using geostatistical approach. *Environ. Monit. Assess.* **2009**, *167*, 599–615. [CrossRef]

56. Delhomme, J. Kriging in the hydrosciences. *Adv. Water Resour.* **1978**, *1*, 251–266. [CrossRef]

57. Jena, V.; Dixit, S.; Shrivastava, R.; Gupta, S. Study of pond water quality by the assessment of physicochemical parameters and water quality index. *Int. J. Appl. Biol. Pharm. Technol.* **2013**, *4*, 47–52.

58. Vaiphei, S.P.; Kurakalva, R.M.; Sahadevan, D.K. Water quality index and GIS-based technique for assessment of groundwater quality in Wanaparthy watershed, Telangana, India. *Environ. Sci. Pollut. Res.* **2020**, *27*, 45041–45062. [CrossRef] [PubMed]

59. Rokbani, M.K.; Gueddari, N.; Bouhlila, R. Use of geographical information system and water quality index to assess groundwater quality in El Khairat Deep Aquifer (Enfidha, Tunisian Sahel). *Iran. J. Energy Environ.* **2011**, *2*, 133–144.

60. Brown, R.M.; McClelland, N.I.; Deininger, R.A.; O'Connor, M.F. A Water Quality Index—Crashing the Psychological Barrier. *Indic. Environ. Qual.* **1972**, 173–182. [CrossRef]

61. Richards, L.A. Diagnosis and Improvement of Saline and Alkaline Soils. *Soil Sci.* **1947**, *64*, 432. [CrossRef]
62. Todd, D.K. *Groundwater Hydrology*, 2nd ed.; Wiley: New York, NY, USA, 1980.
63. Wilcox, L.V. *Classification and Use of Irrigation Water (Circular 969)*; US Department of Agriculture: Washington, DC, USA, 1955.
64. Ragunath, H.M. *Groundwater*, 2nd ed.; Wiley Eastern Ltd.: New Delhi, India, 1987.
65. Subramani, T.; Elango, L.; Damodarasamy, S.R. Groundwater quality and its suitability for drinking and agricultural use in Chithar River Basin, Tamil Nadu, India. *Environ. Earth Sci.* **2005**, *47*, 1099–1110. [CrossRef]
66. Doneen, L.D. *Notes on Water Quality in Agriculture. Water Science and Engineering Paper 4001*; University of California: Oakland, CA, USA, 1964.
67. Kelly, W.P. *Alkali Soils-Their Formation, Properties and Reclamation*; Reinhold Publishing: New York, NY, USA, 1951.
68. Parkhurst, D.L.; Apelo, C.A.J. User's Guide to PHREEQC (Version 2)-A Computer Program for Speciation, Batch-Reaction, One-Dimensional Transport, and Inverse Geochemical Calculations. United States Geological Survey. In *Water Resources Investigations*; Report 99-4259; USGS Publications: Washington, DC, USA, 1999.
69. Schoeller, H. La Classification Géochimique des Eaux. 1964. Available online: http://hydrologie.org/redbooks/a064/064002.pdf (accessed on 5 June 2021).
70. Shout, H.; Bouaicha, F.; Merrad, Z. *The Geothermal Resources of Northeast Constantine Comparative Study, Case of the Region of Guelma and Telaghma (Socio-Economic and Legal Impact)*; Université Mentouri Constantine: Constantine, Algeria, 2021; pp. 30–37.
71. Chabour, N.; Dib, H.; Bouaicha, F.; Bechkit, M.A.; Nacer, N.M. A conceptual framework of groundwater flowpath and recharge in Ziban aquifer: South of Algeria. *Sustain. Water Resour. Manag.* **2021**, *7*, 1–15. [CrossRef]
72. Meybeck, M. Global chemical weathering of surficial rocks estimated from river dissolved loads. *Am. J. Sci.* **1987**, *287*, 401–428. [CrossRef]
73. Mayo, A.L.; Loucks, M.D. Solute and isotopic geochemistry and ground water flow in the central Wasatch Range, Utah. *J. Hydrol.* **1995**, *172*, 31–59. [CrossRef]
74. Cerling, T.E.; Pederson, B.L.; Von Damm, K.L. Sodium-calcium ion exchange in the weathering of shales: Implications for Global Weathering Budgets. *J. Geol.* **1989**, *17*, 552–554. [CrossRef]
75. Fisher, R.S.; Mullican, W.F., III. Hydrochemical evolution of sodium-sulfate and sodium-chloride groundwater beneath the northern Chihuahuan Desert, Trans-Pecos, Texas, USA. *Hydrogeol. J.* **1997**, *5*, 4–16. [CrossRef]
76. McLean, W.; Jankowski, J.; Lavitt, N. Groundwater quality and sustainability in an alluvial aquifer, Australia. In *Ground-Water: Past Achievements and Future Challenges*; Balkema: Rotterdam, The Netherlands, 2000; pp. 567–573, ISBN 90-5809-159-7.
77. Gaillardet, J.; Dupré, B.; Louvat, P.; Allègre, C. Global silicate weathering and CO2 consumption rates deduced from the chemistry of large rivers. *Chem. Geol.* **1999**, *159*, 3–30. [CrossRef]
78. Stuyfzand, P.J. Base exchange indices as indicators of salinization or freshening of (coastal) aquifers. In Proceedings of the 20th Salt Water Intrusion Meeting, Naples, FL, USA, 23–27 June 2008.
79. Appelo, C.A.; Postma, D. *Geochemistry, Groundwater and Pollution*; Balkema: Rotterdam, The Netherlands, 1993.